

**Chapter 4:**  
**The role of kinetochose**  
**proteins in the development**  
**and virulence of**  
*Magnaporthe oryzae*



#### **4. Chapter 4: The role of kinetochore proteins in the development and virulence of *Magnaporthe oryzae***

The structure and assembly of kinetochore subunits is crucial to its function and differs across systems. Studying the dynamics of kinetochore proteins provides information regarding the order and timing of the assembly of different sub-complexes at the centromere. I tagged the DASH complex proteins Dam1 and Ask1, separately, with GFP (green fluorescent protein) to study the subcellular localisation patterns and cell-cycle associated dynamics of outer kinetochore proteins. In order to study the localisation of the proteins with respect to the chromosomes, both proteins were tagged in a strain expressing histone H1-mCherry (hH1-mCherry). Dam1 was tagged on the N-terminus while Ask1 was tagged on the C-terminus, as described in chapter 3. As a marker for the kinetochore, the localisation of the middle kinetochore Mtw1/MIND Complex protein Mis12 was also studied. Mis12 was tagged with GFP on the C-terminus in the hH1-mCherry background strain.

##### **4.1 Mis12 is associated with the nucleus during interphase**

In vegetative hyphae, 92% of the interphase cells analysed showed a single distinct Mis12-GFP puncta in association with the nucleus, mostly close to the periphery (arrowhead; Fig. 4.1). *M. oryzae* has seven chromosomes. The presence of a single Mis12 spot indicates centromere/kinetochore clustering during interphase. This clustering is a common feature shared among ascomycete yeasts, previously described in *S. cerevisiae*, *C. albicans* and *S. pombe*. In *S. cerevisiae* and *C. albicans* the clustering is maintained throughout the cell cycle, while *S. pombe* kinetochores de-cluster during mitosis. The dynamics are reversed in the basidiomycete pathogenic yeast *C. neoformans* where kinetochores are not clustered during interphase, but begin to cluster at the onset of mitosis (Kozubowski et al., 2013). Further, *C. neoformans* shows ordered

kinetochore assembly with only the inner kinetochore proteins Cse4 and Mif2 present at unclustered kinetochores and the middle (Mtw1 and Nuf2) and outer (Dad1 and Dad2) layers assembled during mitosis at clustered kinetochores (Kozubowski et al., 2013). In *A. nidulans*, the kinetochores are clustered during interphase and de-cluster during mitosis similar to *S. pombe* (De Souza et al., 2009; Funabiki et al., 1993; Yang et al., 2004). Most metazoans, except in a few tissues at certain stages of development, rarely show clustering of kinetochores at any stage of the cell cycle.

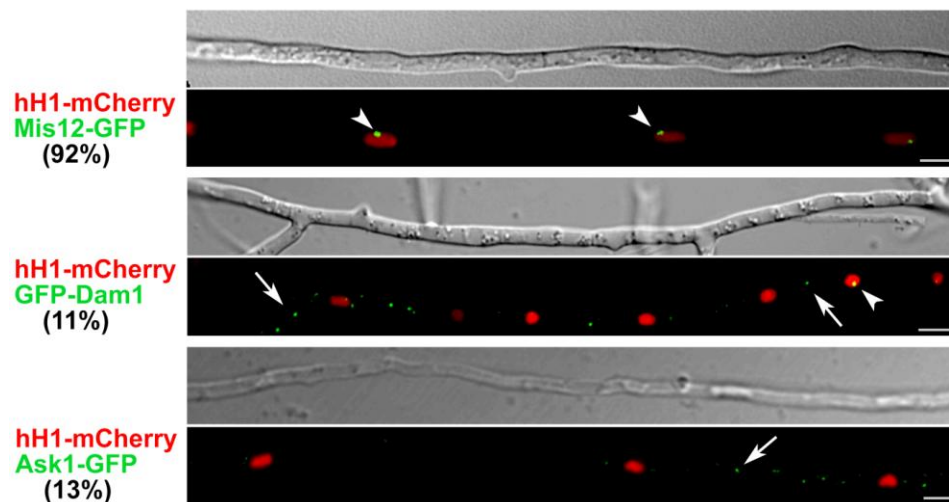


**Figure 4. 1: Subcellular localisation of kinetochore proteins during interphase**

Localisation of middle (Mis12-GFP,  $n = 207$ ) and outer (GFP-Dam1,  $n = 207$  and Ask1-GFP,  $n = 227$ ) kinetochore proteins during interphase in vegetative hyphae. Numbers indicate percentage of nuclei with associated KT proteins during interphase. Arrowheads indicate nuclear-associated Mis12-GFP or GFP-Dam1 or Ask1-GFP. Arrows denote GFP-Dam1 or Ask1-GFP spots probably associated with cytoplasmic microtubules. Scale bar = 5  $\mu\text{m}$ .

During interphase, the *S. pombe* centromere cluster appears as a single dot attached to the nuclear envelope in close proximity to or overlapping with the spindle pole body. The tethering of centromeres to the nuclear envelope near the SPB region during interphase is facilitated by SUN/KASH domain proteins like Sad1, and its interacting nuclear protein

Csi1 in *S. pombe* (Hou et al., 2012). Kinetochore clustering favours rapid chromosome capture at the onset of mitosis, and lack of clustering leads to mitotic delays. The location of the *M. oryzae* kinetochore cluster at the nuclear periphery (Fig. 4.1) is probably maintained through an association with the nuclear envelope. Determination of whether the cluster lies in the proximity of the SPB will require co-localisation studies with SPB markers like Spc42, Sid4 or  $\gamma$ -tubulin.

In contrast to Mis12, the Dam1 and Ask1 subunits of the DASH complex rarely associated with the interphase nucleus, only 11-13% cells showing nuclear-associated signal (arrowheads, Fig. 4.1, middle and lower panels). Instead, cytoplasmic punctae of Dam1 and Ask1 were seen in vegetative hyphae (arrows; Fig. 4.1), especially in the hyphal tip cell. Owing to the known microtubule association of the complex, these were DASH complex proteins presumably associated with cytoplasmic microtubules.

*M. oryzae*, as described earlier, produces many different types of cells during its lifecycle. To see if the localisation pattern was specific to vegetative hyphae or was a constant feature of the *M. oryzae* interphase, I looked at the localisation of the kinetochore proteins during the different developmental stages. Similar nuclear association of Mis12-GFP punctae was seen in conidia, conidiophore, appressoria and invasive hyphae during interphase (Fig. 4.2 and 4.4). The Mis12-GFP puncta associated with the nucleus at all stages of conidiation- 1-cell, 2-cell and in mature three-cell stage as well as in the conidiophore (Fig. 4.2A, B). Occasionally, conidial cell nuclei (~10%) did not display an associated Mis12-GFP spot, at a frequency similar to that observed in vegetative hyphae. Absence of a single distinct puncta may occur briefly when the subunits dissociate from the centromere during DNA replication.

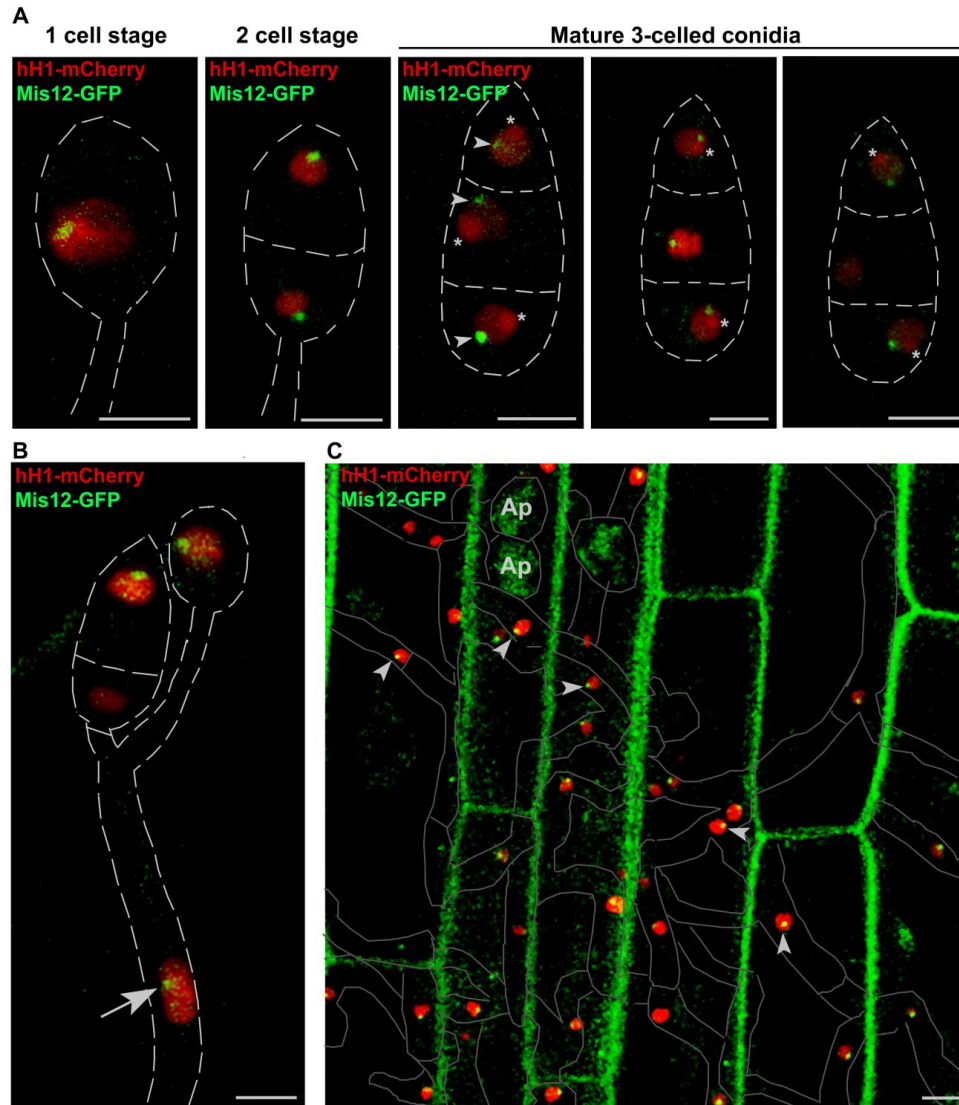


**Figure 4.2: Mis12 is associated with the nucleus during interphase**

Subcellular localisation of Mis12-GFP in A) conidia, B) conidiophore and C) invasive hyphae. Outlines indicate fungal structures. Arrowheads mark nucleus-associated Mis12-GFP spots. Asterisks mark the nucleolar regions of the nucleus. Appressoria are indicated as Ap. Arrowheads mark nucleus-associated Mis12-GFP in the conidiophore. Scale bar = 5 μm.

Through most of interphase, the nucleolus is visible as an intense circular region within the nucleus (mature conidia; Fig. 4.2A). I asked whether there was any correlation between the nucleolus and the Mis12-GFP spot. In some cases, the Mis12-GFP spot was seen associated to the nucleolus

or present in its proximity, while on other occasions it was seen away, suggesting no clear pattern or correlation between the two structures (Fig. 4.2A, mature conidia). In budding yeast, the nucleolus is present diametrically opposite to the SPB during interphase in actively growing cells, while the SPB may deviate from this central axis during quiescence or unfavourable nutrient conditions (Yang et al, 1989, Wang et al, 2016). Irrespective of the nucleolus position, the Mis12-GFP spot was always observed close to the nuclear periphery in *M. oryzae*.

In addition to the intense nucleus-associated Mis12-GFP spot, I occasionally also observed a diffuse GFP signal in the nuclei of conidia (Fig. 4.2A). A dispersed Mis12 signal has been observed in the nuclei of human cell lines. In yeast, though Mis12 is constantly associated with the centromere, the levels change through the course of the cell cycle. This likely occurs through a turnover and exchange with the nuclear pool which may contribute to the diffuse nuclear signal seen in *M. oryzae*. I also observed nuclear associated Mis12-GFP spots in invasive hyphae infecting rice sheaths (Fig. 4.2C).

Similar to the localisation in vegetative hyphae, GFP-Dam1 rarely associated with the nuclei even in conidia and appressoria (Fig. 4.3 and 4.5). In conidia, GFP-Dam1 was seen as many extremely weak small spots distributed all over the conidium. Though spots were seen in the vicinity of the nucleus, hardly any nuclei showed the tight association seen with Mis12. Interestingly, the apical cell of the conidium often showed more GFP-Dam1 spots (Fig. 4.3). The apical cell, the youngest cell of the conidium, germinates ~70% of the times, and likely has the most dynamic MT network, and the GFP-Dam1 spots may be associated with the cytoplasmic MTs. All in all, irrespective of the developmental stage, Mis12 is associated with nucleus during interphase, while outer kinetochore proteins Dam1 and Ask1 are observed in the cytoplasm.

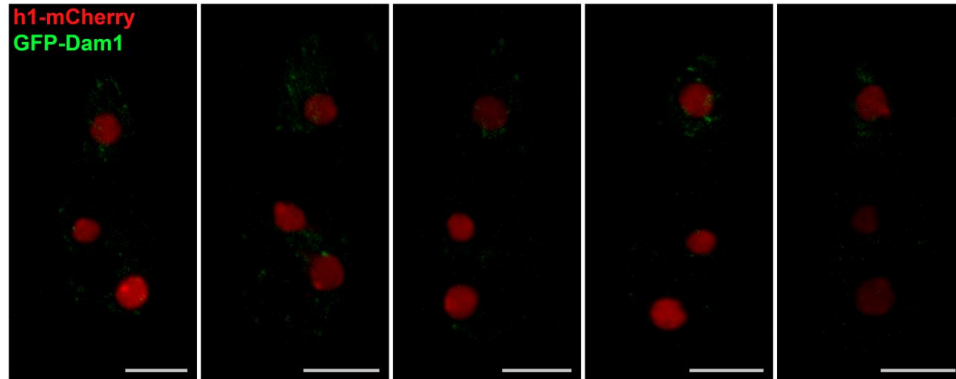


**Figure 4.3: Cytoplasmic localisation of GFP-Dam1 in conidia**

Subcellular localisation of GFP-Dam1 in mature three celled conidia. Scale bar = 5  $\mu\text{m}$ .

#### **4.2 Outer kinetochore DASH complex proteins Dam1 and Ask1 associate with the nucleus during mitosis**

I monitored mitosis in the actively growing and dividing tips of hyphae. Generally, nuclei in hyphal tip cells appear oblong, as they continuously migrate towards the cell centre as the cell grows in length. In *M. oryzae*, the cells are longest at the hyphal tip and become smaller away from it, showing a more circular nucleus. In fungi, such nuclear morphologies have been suggested to maintain a constant nucleo-cytoplasmic ratio (Jorgensen et al., 2007; Neumann and Nurse, 2007). The nucleus in the *M. oryzae* tip cell shows a uniform homogenous histone signal that dips in intensity prior to mitosis. This is probably due to the semi-closed mitosis *Magnaporthe* undergoes, where for a brief period during mitosis nuclear proteins are freely exchanged with the cytoplasm, through pores in the nuclear envelope (Jones et al., 2016). GFP-Mis12 was associated with the nucleus much prior to mitosis, and is generally seen towards the front end of the nucleus migrating in the direction of the tip of the hyphal cell (red arrow, Fig. 4.4). The apical cell grows to approximately twice the length of the sub-apical cell before division. This was used as an indicator to identify cells likely to enter mitosis.

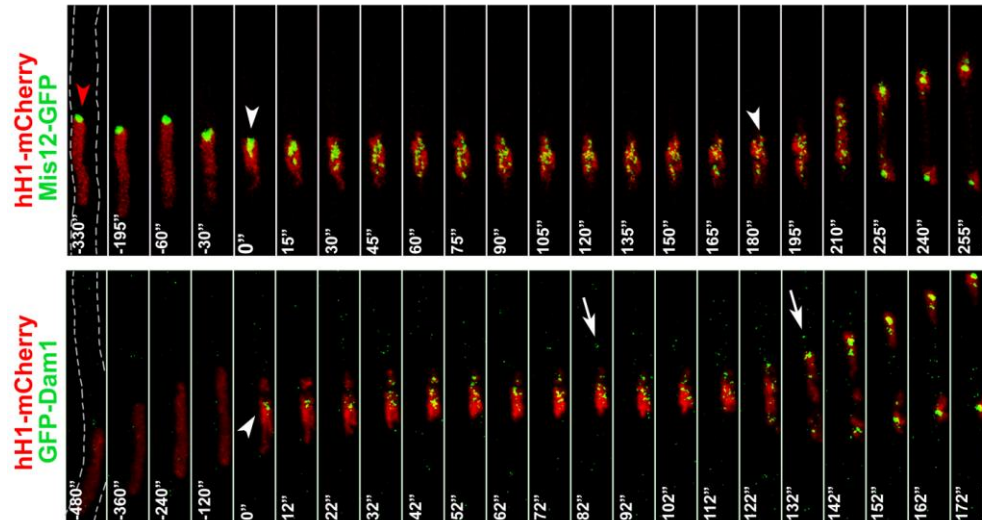


**Figure 4.4: Outer kinetochore protein Dam1 associates with the nucleus during mitosis**

Time-lapse images showing dynamics of Mis12-GFP and GFP-Dam1 during mitosis in vegetative hyphae,  $n = 10$ . Numbers indicate time in seconds. Fungal structures are marked with dashed outlines. Arrowheads indicate nuclear-associated Mis12-GFP or GFP-Dam1. Red arrowhead indicates Mis12-GFP associated with the nucleus prior to mitosis. Arrows denote GFP-Dam1 spots probably associated with cytoplasmic microtubules along the vegetative hyphae. Scale bar = 3  $\mu\text{m}$ .

The onset of mitosis was marked by loss of the typical circular/ oval nuclear structure and the appearance of condensed chromosomes. As the chromosomes condensed, the single Mis12-GFP puncta (associated with the nucleus) de-clustered into multiple foci and multiple GFP-Dam1 punctae appeared at the nucleus. During mitosis, GFP-Dam1 punctae appeared at the nucleus and stayed through nuclear migration, often remaining linked to the nuclei even after they had reached their positions (arrowheads, Fig. 4.4). As mitosis progressed towards anaphase, the Mis12-GFP spots further increased in number (likely doubled) from what was seen at the start of mitosis, probably due to chromatid separation. At the end of mitosis, the nucleus also acquired the more compact typical oval structure and each nucleus was associated with a single large Mis12-GFP and GFP-Dam1 puncta formed by the re-clustering of the individual

kinetochores (Fig. 4.4). Thus the few cells that showed a nuclear-associated GFP-Dam1 spot during interphase (~11-13%) as observed earlier (Fig. 4.1), were likely cells that had recently undergone mitosis.

The *S. cerevisiae* Dam1 complex proteins associate with the centromere/KT through the entire cell cycle, while components of the DASH complex in *S. pombe* DASH proteins are recruited to the KT during mitosis, except for Dad1. In *M. oryzae* I observed that Dam1 associated with the nucleus at the start of mitosis coincidentally with chromosome condensation and the interaction was maintained during the separation of chromosomes and nuclear migration. The MIND complex protein Mis12, on the other hand behaved as a constitutive kinetochore component of the kinetochore, maintaining nuclear association through the complete cell cycle, likely dissociating only during replication of centromeric DNA. These single spots of Mis12 observed during interphase, resolved into multiple smaller foci during nuclear division, highlighting the dynamic nature of both the reference protein as well as KT clustering. The *M. oryzae* kinetochore protein dynamics align with those described in *S. pombe* and *A. nidulans*, where KTs are de-clustered during metaphase (Goshima et al., 1999), in contrast to the budding yeasts, where declustering of centromeres is not visible even during mitosis (Roy et al., 2011).

In addition, there is considerable flexibility in the number of copies of Mis12 and NDC80 protein complexes that associate with the kinetochore in *S. cerevisiae* across the different cell cycle phases. The tightly attached ‘anaphase configuration’ is achieved by further assembly of several copies of the complexes onto the KT of the ‘G1 configuration’ (Dhatchinamoorthy et al., 2017). The dynamic KT structure is probably best suited to maintain more stable attachment during segregation of chromosomes in anaphase, while permitting easy correction of erroneously attached chromosomes prior to biorientation. Future quantitative investigation will throw light on whether *M. oryzae*

demonstrates any such structural plasticity and whether the findings hold true for other filamentous fungi. In my experience, the pre-mitotic nucleus-associated Mis12 cluster was bigger than that seen after chromosome segregation in *M. oryzae* (Fig. 4.1B). This may occur due to the presence of a duplicate set of kinetochores associated with each nucleus (14 in *M. oryzae*) during mitosis or re-inforcement of the structure with additional copies of Mis12 in preparation for mitosis.

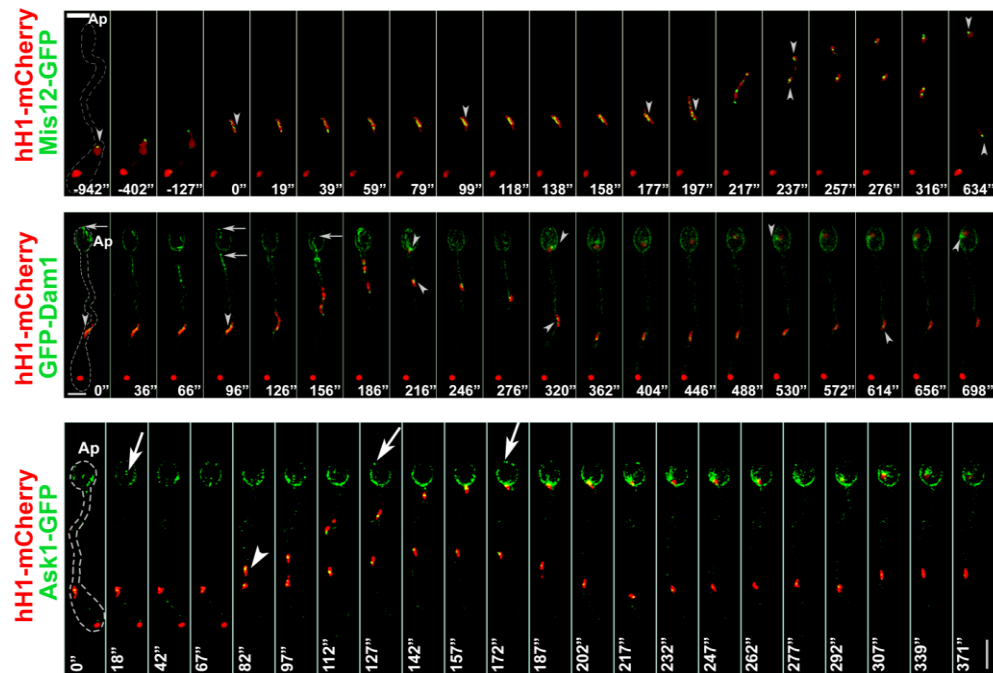


**Figure 4.5: Dam1 associates with the nucleus at mitotic onset in *M. oryzae* during appressorium development**

Time-lapse images showing dynamics of middle (Mis12-GFP) and outer (GFP-Dam1 and Ask1-GFP) kinetochores proteins during appressorium (Ap) development,  $n = 5$ . Numbers indicate time in seconds. Fungal structures are marked with dashed outlines. Arrowheads indicate nuclear-associated Mis12-GFP or GFP-Dam1 or Ask1-GFP. Arrows indicate non-nuclear spots of GFP-Dam1 or Ask1-GFP in the appressorium. Scale bar = 5  $\mu\text{m}$ .

To assess Dam1 dynamics during the early pathogenic events in *M. oryzae* and identify any differences from patterns described above in vegetative

growth, I studied the localisation of GFP-Dam1 during the formation of the dome-shaped appressorium, the infection structure responsible for disrupting the rice leaf cuticle. In order to find out whether the localisation pattern was not specific to Dam1 but shared by other DASH complex proteins, I also included Ask1-GFP in the analysis. During appressorium formation, nuclear-association of Ask1-GFP and GFP-Dam1 was observed at the time of nuclear division and migration (Fig. 4.5). While no non-nuclear Mis12-GFP signal was observed during mitosis, GFP-Dam1 and Ask1-GFP were observed along the germ tube and appressorium, likely associated with non-kinetochore spindle microtubules and MTs involved in tethering the nucleus to the cell cortex, during nuclear migration.

Thus, during both vegetative as well as pathogenic development of *M. oryzae*, Mis12 the middle KT protein constitutively associated with the kinetochore, while the outer kinetochore proteins, in this case DASH complex proteins, showed mitosis-specific association with the nucleus. In summary, the cell cycle dynamics of middle and outer kinetochore proteins studied here in *M. oryzae* show behaviour more similar to that reported in *S. pombe* than in budding yeasts or mammalian systems.

Next, to investigate the role of the DASH complex proteins during mitosis, I looked at spindle dynamics and chromosome segregation in the absence of Dam1. I generated *DAM1* deletion strains, in the WT B157 strain and the hH1-mCherry and Tub-GFP tagged strain (as described in Chapter 3), hereafter referred to as *dam1* $\Delta$ . I deleted *ASK1* in the strain expressing GFP-Dam1 (hereafter referred to as *ask1* $\Delta$ ).

### **4.3 Dam1 is crucial to proper spindle structure and segregation of chromosomes**

Changes in subcellular patterns of the nuclei (hH1-mCherry) and the microtubule network ( $\beta$ -Tubulin-sGFP) associated with mitosis were studied during vegetative hyphal growth in *M. oryzae* (Fig. 4.6). At the start of mitosis in the WT strain chromosome condensation, characteristic

of prophase, occurred. Microtubule re-organisation was characterised by a concurrent loss of the network of cellular microtubules and establishment of a distinct focal point in association with the the chromosomes, probably at the spindle pole body (or nuclear MTOC) which is known to act as a site for spindle microtubule nucleation during mitosis.

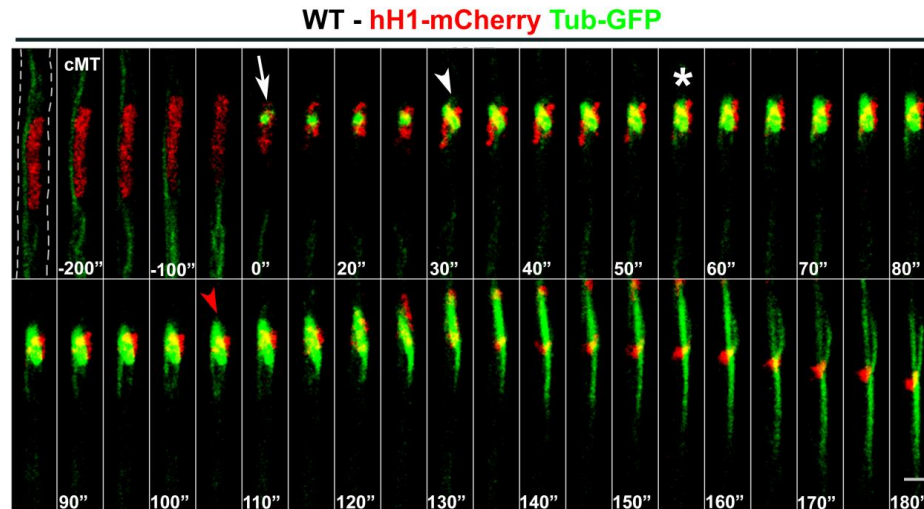


**Figure 4.6: Dynamics of the mitotic spindle in WT *M. oryzae***

Time-lapse images of formation and elongation of the spindle during mitosis in vegetative hyphae. The MTs and chromosomes are marked with Tub-GFP and hH1-mCherry. Numbers indicate time in seconds. Hyphal borders are indicated with dashed lines. Arrow depicts entry into mitosis, arrowhead indicates assembly of a bipolar spindle, asterisk shows spindle re-orientation, and red arrowhead indicates onset of spindle elongation. Scale bar = 3  $\mu$ m. cMT, cytoplasmic MTs.

Next, I observed the assembly of the bipolar spindle as a short intense bar which eventually aligned along the long axis of the hypha. The spindle maintained a more or less fixed length through metaphase until spindle elongation during anaphase. Anaphase A was marked by separation of the chromosomes, followed by spindle elongation in anaphase B. Spindle elongation was frequently initiated within 3 minutes (Fig. 4.7C). The segregated chromosomes then formed two daughter nuclei that migrated to opposite ends in telophase (Fig. 6). The *dam1* $\Delta$  strain displayed longer

spindles ( $5.37 \pm 0.16 \mu\text{m}$ ) in the absence of Dam1 function compared to the WT ( $3.71 \pm 0.07 \mu\text{m}$ ) (Fig. 4.7B). Further, the *dam1* $\Delta$  mutant occasionally showed altered spindle structure (MTs emanating from a single pole, or bipolar spindles with MTs directed away from the two poles, or an additional focal point or pole), with some instances of collapsed spindles. Similar phenotypes have been observed in budding yeast, with different *dam1* mutants as well as mutants of other DASH complex proteins showing a range of spindle defects including elongated, hyperelongated or extremely short spindles.

Spindle length is maintained through a balance of inward and outward forces (Goshima and Scholey, 2010). Any disruption of these forces alters spindle length, with higher inward forces leading to a shorter spindle and higher outward forces leading to an elongated spindle. Constant spindle length is achieved through equilibrium of opposing forces generated by motor proteins, where minus end motors like dynein and kinesin-14 exert a pulling or inward force while kinesin-5 exerts an outward or pushing force. Further, mutations or overexpression of budding yeast motor proteins, such as Kar3 (Kinesin-14 family; Klp2 in *S. pombe*), Cin8, Kip1 (kinesin-5) and Kip3 (Kinesin-8 family; Klp5/Klp6 in *S. pombe*) which are involved in microtubule network integrity and dynamics, affect the length of the mitotic spindle (Straight et al., 1998, Zeng et al., 1999). Overexpression of Kar3 leads to shorter spindles while overexpression of Cin8 leads to longer spindles. Further, many microtubule associated proteins regulate microtubule dynamics and length, which also affect spindle length. Cohesins, which bind sister chromatids, generate an inward force, preventing spindle elongation. Further, chromosomal attachments generate an inward force, and the inward force is likely proportional to the number of attached kinetochores.

Thus, absence of chromosomal attachments leads to longer spindles. Dam1 is known to facilitate spindle MT depolymerisation as well as being involved in KT-MT interactions in yeast.

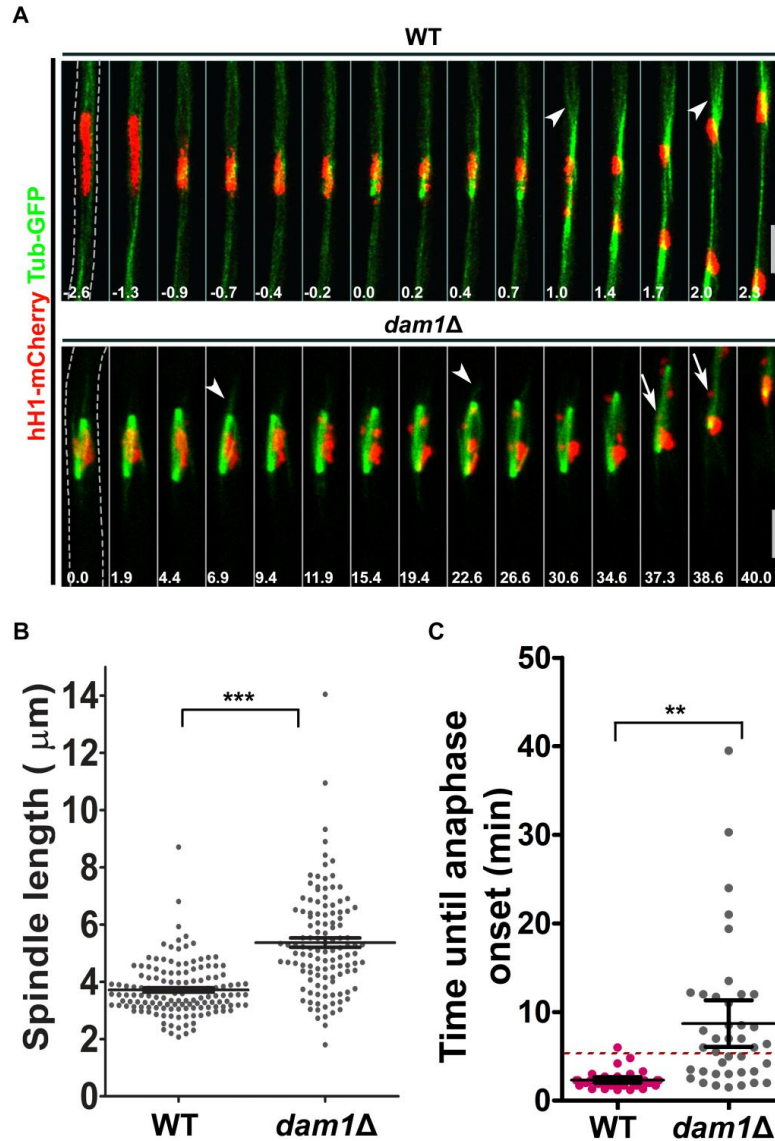


**Figure 4.7: Dam1 alters spindle structure and dynamics**

Dam1 plays an important role in proper segregation of chromosomes during nuclear division. A) Time-lapse images of mitosis in the WT or *dam1Δ* vegetative hyphae. Numbers indicate time in minutes. Hyphae are marked with dashed outlines. Arrowheads indicate astral MTs and arrows show lagging chromosomes. Scale bar = 5  $\mu\text{m}$ . B) Scatter Plot showing mean  $\pm$  s.e.m. spindle length in the WT (n=143) or *dam1Δ* (n=119) strains during mitosis. \*\*\* $P < 0.001$ , two-tailed  $t$  test. C) Scatter Plot showing mean  $\pm$  s.e.m. time until spindle elongation in anaphase in WT or *dam1Δ* strains during mitosis in vegetative hyphae. \*\*\* $P < 0.001$ , two-tailed  $t$  test, n = 40.

Thus, I suspect that the elongated mitotic spindles in *dam1Δ* are either due to altered microtubule dynamics or lack of proper chromosomal-MT attachments or a combination of both. With the current information it is not possible to rule out any one reason.

To investigate this further, I monitored spindle dynamics in the *dam1Δ* strain with reference to the WT (Fig. 4.7A). I found that the the WT and *dam1Δ* strains spindle was maintained for different durations until the onset of anaphase. Spindle elongation in the *dam1Δ* mutant was delayed considerably compared to the WT (Fig. 4.7D). In the WT, chromosome segregation mostly started within 3 minutes ( $2.31 \pm 0.15$  mins), whereas many *dam1Δ* mutant spindles persisted for over 10 minutes ( $8.70 \pm 1.29$  mins) until anaphase was initiated (Fig. 4.7 A, D). The *dam1Δ* strain showed significant inter-cellular heterogeneity with regard to time spent before spindle elongation (3-39 minutes), in which a few cells showed dynamics similar to WT, while others took much longer to initiate anaphase (Fig. 4.7D). Improper segregation of chromatin masses or lagging chromosomes trailing behind the rest were seen in a few cells of *dam1Δ* (arrows, Fig. 4.7A). The delay in anaphase onset is likely due to the activation of the spindle assembly checkpoint which prevents spindle elongation until bi-orientation of all sister chromatids is achieved.

I looked at the chromosome and spindle dynamics in *dam1Δ* in detail (Fig. 4.8), and found that the chromosomes were highly dynamic for a very long time, indicating that bi-orientation had not been achieved. There was considerable fluctuation in spindle length even for a given cell, that exceeded the average spindle length in the WT, and several unattached MTs, likely in search of chromosomes, were seen even several minutes after spindle establishment. The spindle length reduced towards the end of mitosis and the chromosomes were placed in the middle half of the spindle, just prior to elongation, possibly due to establishment of proper KT-MT interactions that allowed mitosis to proceed.

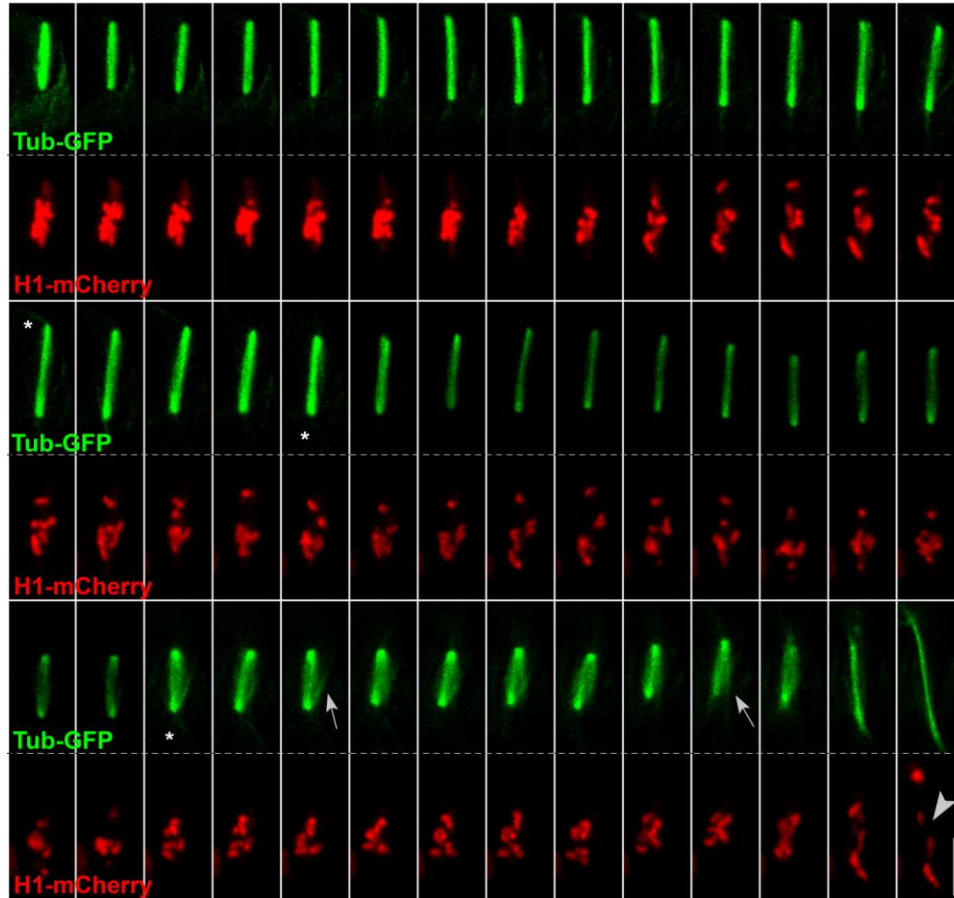


**Figure 4.8: Spindle and chromosome dynamics during a prolonged metaphase in *dam1*Δ**

Time-lapse images of chromosome and spindle dynamics during mitosis in *dam1*Δ vegetative hyphae. Images are at intervals of 15 seconds. Asterisks mark astral MTs. Arrows indicate unattached or searching MTs and arrowhead show lagging chromosomes. Scale bar = 5 μm.

Further the chromosomes were distributed all along the length of the spindle, sometimes even close to the poles, likely making it difficult for chromosome capture to occur, suggesting that bi-orientation had not been achieved until very late. Thus, Dam1 is vital for maintenance of spindle structure and integrity over and above establishment of proper KT-MT interactions to achieve chromosome bi-orientation in *M. oryzae*. Dam1 function is thus important for metaphase spindle structure and chromosome segregation at anaphase, allowing proper mitotic progression during vegetative (hyphal) growth in *M. oryzae*.

#### 4.4 Polarised growth is dependent on proper DASH complex function

Subsequently, I enquired whether *Magnaporthe* development was affected in absence of Dam1 function. Colony diameter of *dam1Δ* strains was reduced to 60% of the WT colony (Fig. 4.9A, B). The growth defects shown here on prune agar (Fig. 4.9A), were consistently also observed on YEG (yeast extract glucose) medium, oatmeal agar, basal medium and complete medium, and hence were not due to any unfavourable nutrient conditions.

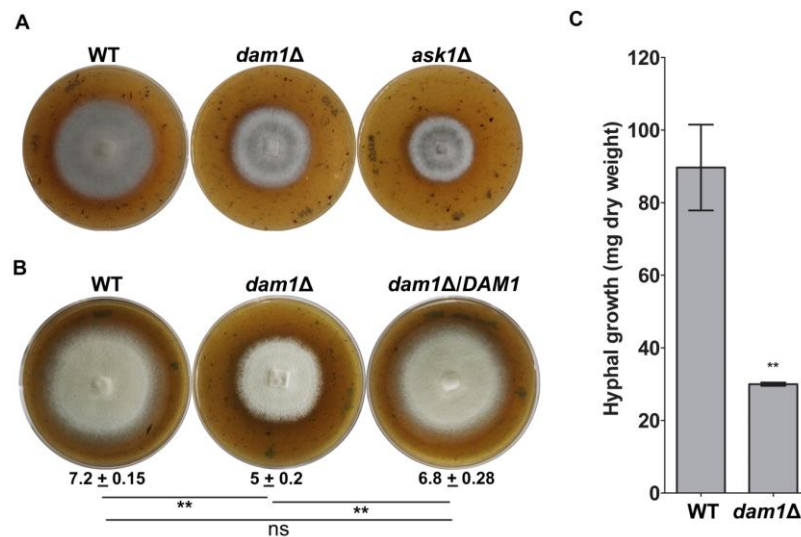


**Figure 4.9: The DASH complex is involved in hyphal growth**

A) Vegetative growth of WT, *dam1Δ* and *ask1Δ* strains at 9 dpi on prune agar. B) Vegetative growth of WT, *dam1Δ* and *dam1Δ/DAM1* strains at 10 dpi on prune agar. Numbers indicate mean  $\pm$  S.E.M. colony diameter in centimetres from three independent experiments with  $n=3$  each. \*\* $P<0.05$ ; ns, not significantly different; two-tailed  $t$  test. C) Increase in Dry weight of WT and *dam1Δ* hyphal biomass at 4 dpi in complete medium broth.

Next, I asked whether the growth defect was specific to Dam1 or extended to the other member of the complex, Ask1. *ask1Δ* also showed similar hyphal growth defects and reduced colony diameter (Fig. 4.9A). To confirm that the growth defects seen in *dam1Δ* were due to loss of Dam1 and nothing else, we complemented the mutant strain with *GFP-DAM1*.

Radial hyphal growth was restored to WT colony diameter by complementation of *dam1Δ* with *DAM1* (Fig. 4.9B). When the *M. oryzae* cultures were maintained for long periods of time, the *dam1Δ* mutant did not recover or draw level with the WT even at later time points. Since colony diameter only takes into account two-dimensional substratum-associated hyphal growth, I looked at hyphal biomass grown in liquid medium. Increase in dry weight of *dam1Δ* mutant hyphal biomass grown in liquid complete medium was only 40% of the WT (Fig. 4.9C). An important aspect of *M. oryzae* hyphal development is the extension of aerial hyphae. I checked whether the growth defect extended to aerial hyphae. The *dam1Δ* mutant showed sparse aerial hyphae, producing rather flat colonies compared to the dense growth seen in the WT. Thus, the *dam1Δ* mutant displays a hyphal growth defect irrespective of the growth conditions and the nature of hyphae.

Branching is central to the development of fungal colonies, increasing the surface area and facilitating nutrient acquisition. Hyphal branching follows two major patterns-apical and lateral- and is regulated by internal factors as well as external cues (Harris, 2008; Harris, 2019). The modular nature of fungal colonies allows the differentiation of the hyphal cells, with the apical (tip) cell involved in nutrient assimilation and environment sensing and sub-apical cells providing new hyphae by lateral branching. Lateral branching is the predominant branching pattern observed in fungi and most often does not affect the growth rate at the hyphal tip. Normally individual hyphae display a phenomenon known as apical dominance which suppresses branching in the vicinity of the hyphal tip, likely through the exclusive delivery of the exocytic vesicles to the hyphal tip, and branching is only observed a considerable distance away from the tip.

Apical branching (also known as dichotomous branching or tip splitting), refers to the emergence of a branch from the hyphal tip and has been observed in many fungi. It is generally seen in response to reduced growth rates at the tip without affecting vesicle transport, leading to accumulation

of exocytic vesicles at the tip. Several mutations in *A. nidulans* and *N. crassa* cause apical branching. However, apical branching is common in wild isolates of other fungi, and therefore does not represent only a defect, but rather an alternate branching pattern. *Ashbya gosypii*, for instance, initially displays lateral branching at slower growth rates, until a certain threshold growth rate is achieved, and then switches to apical branching in a process known as hyphal maturation. Within lateral branching, two patterns are seen, branches associated with septa and random branching. In the first case, new branches often emerge just behind the septa, likely due to obstruction of any further vesicle transport. However, mutants that affect chitin deposition or cause actin mislocalisation suggest that there are several other factors involved and the above explanation is too simple. While *A. gosypii* and certain basidiomycetes show branching adjacent to septa, *N. crassa* and *A. nidulans* from the Pezizomycota class of ascomycetes display random branching. In *N. crassa*, branches emerge from the centre of sub-apical cells, while *Aspergillus* has a slight bias for the apical septum. Thus, septum formation seems to define branch points, albeit to varying degrees. Therefore, though there is some understanding about branching patterns, what mechanisms determine selection of branching sites still remains a very open question in fungal biology.

In *M. oryzae*, vegetative hyphae grow in a monopolar manner with apical extension and lateral branching, with branches emerging at fairly long distances from the hyphal tip (Fig. 4.10A). The WT hyphae branched at fairly regular intervals, at acute angles to the primary hypha (Fig. 4.10). The branches often emerged in the proximity of the septum that marked the cell boundary towards the growing tip. Two adjacent branches were often separated by an interval of 2-3 cells.

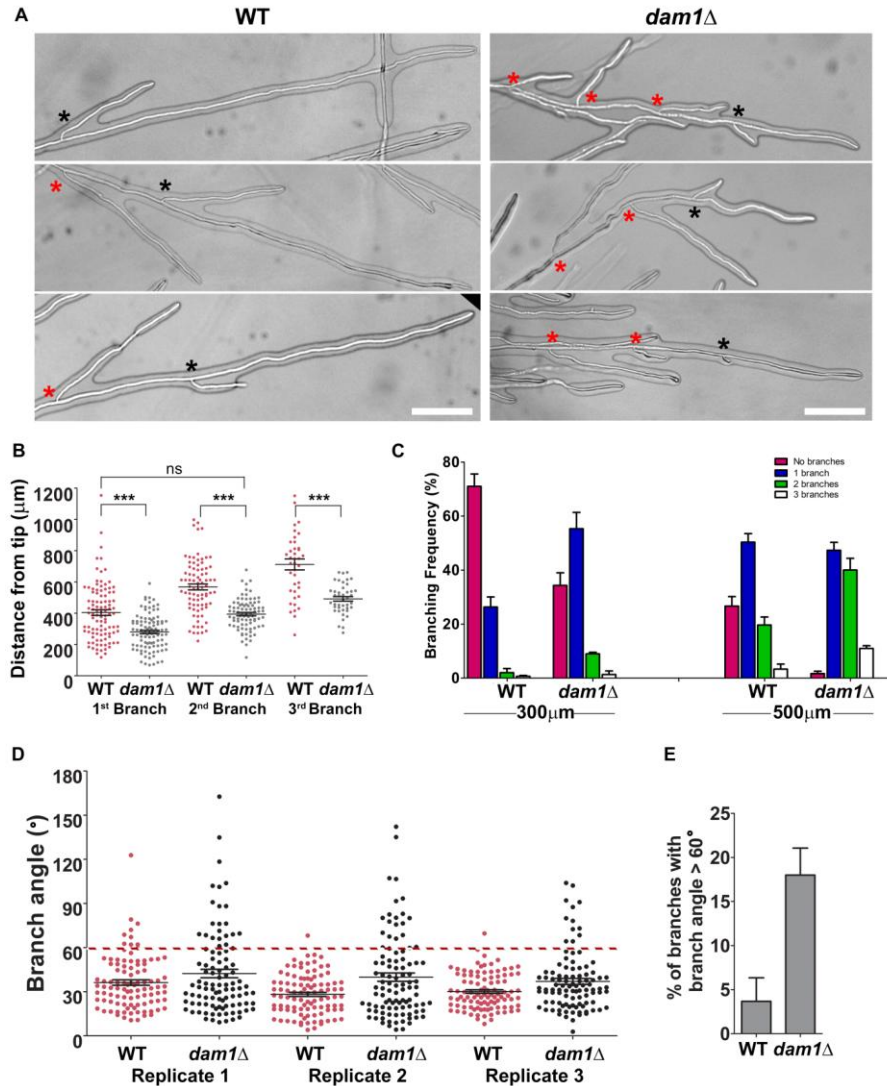


**Figure 4.10: Altered branching pattern in the absence of Dam1 function**

A) Differences in the branching pattern of vegetative hyphae in the WT and *dam1*Δ strain. Black asterisks indicate first branch from the tip. Red asterisks indicate all subsequent branches. Scale bar = 100  $\mu\text{m}$ . B) Scatter plot showing mean  $\pm$  S.E.M. distance of first (n=100), second (n=80) and third branch (n=40) from the apical tip in the WT and *dam1*Δ vegetative hyphae from three independent experiments. \*\*\*P<0.001; ns, not significantly different, two-tailed t-test. C) Branching frequency indicated as % of hyphae with no, 1, 2 or 3 branches within a distance of 300  $\mu\text{m}$  or 500  $\mu\text{m}$  from the growing tip in the WT and *dam1*Δ strain. Data show mean  $\pm$  S.E.M. from three independent experiments, n = 100. D) Branching angles with reference to the primary hypha in the WT and *dam1*Δ strain. The scatter plot shows distribution of data from three

replicates, n = 100. E) Frequency of branch angle greater than 60° in the WT and *dam1Δ* strain, n = 100,  $P < 0.05$ . Data show mean  $\pm$  S.E.M. from three independent experiments.

Studies in *A. nidulans* and *C. albicans* suggest a coordination of branching with the cell cycle, such that the sub-apical cell accumulates sufficient cytoplasmic material before branch emergence and nuclear division. Several environmental factors also seem to affect branching patterns, and certain examples have been observed in interactions with plants. For example, mycorrhizal fungi like *Glomus* normally display apical dominance that switches to profuse branching in presence of root exudates from the host, eg. in response to strigolactones. Similar switches in hyphal patterning have been observed during early development of lichens in association with algal cells. Likely, such regulated switches in hyphal patterning are also involved in *Magnaporthe*, where the germ tube is unbranched and aseptate prior to host invasion, whereas, the invasive hyphae growing within the leaf tissue show profuse branching.

The *dam1Δ* strain branched profusely (Fig. 4.10A-C). Within the distance from the hyphal tip in which the WT produces one branch, two branches are formed in the *dam1Δ* (Fig. 4.10B). The *dam1Δ* branches emerged at ~70% of the distances of their WT counterparts from the hyphal tip (Fig. 4.10B). Excessive branching has been previously observed in *M. oryzae* in the mutant of MoSpa2, a polarity factor (Li et al., 2014). Further, WT branches emerged at fairly uniform angles, reducing the chances of branches running into each other and competing for nutrition. However, compared to WT, *dam1Δ* showed a more random arrangement of branches with an increased frequency of branch angles exceeding 60° (Fig. 4.10D, E). Rearward branching (reverse to the growth direction of the primary hypha) and tip splitting are unusual in the WT, however these were observed in the absence of Dam1.

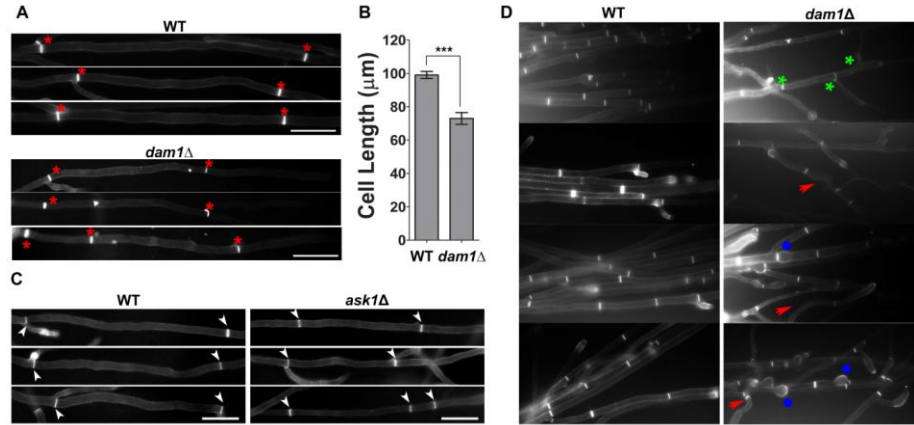


**Figure 4.11: Altered hyphal morphology in absence of DASH complex proteins**

A) Sub-apical cell compartment length in WT and *dam1Δ* vegetative hyphae stained with calcofluor white (CFW). Red asterisks indicate septa (cell boundaries). Scale bar = 20 μm. B) Bar chart showing length of sub-apical cell compartments in the WT and *dam1Δ* vegetative hyphae. Data show mean  $\pm$  S.E.M from three independent experiments. \*\*\* $P < 0.0001$ , *t*-test,  $n = 200$ . C) Sub-apical cell compartment length in WT and *ask1Δ* vegetative hyphae stained with calcofluor white (CFW). Arrowheads indicate septa (cell boundaries). Scale bar = 20 μm. D) Hyphal morphology in WT and *dam1Δ* vegetative hyphae stained with calcofluor white (CFW). Green asterisks indicate branches. Red arrows indicate curved hyphae. Blue dots mark bulged hyphae (irregular hyphal diameter).

Since branching is often associated with septation, and I observed branching at shorter distances, I reasoned that the higher branching frequency might arise from an alteration of the size of cell compartments upon loss of Dam1 function in *M. oryzae*. To address this possibility I stained hyphae with calcofluor white (CFW) and measured the length of the sub-apical compartments. Indeed *dam1Δ* hyphae showed smaller (~70%) compartments than the WT (Fig. 4.11A, B). The *ask1Δ* mutant showed similar defects in septation during vegetative hyphal growth (Fig. 4.11C). Septation probably promotes branching by acting as a barrier to tipward movement of growth tip proteins and exocytic vesicles, leading to their accumulation. Further, *dam1Δ* hyphae stained with CFW lacked the uniform nature of WT compartments and were often irregularly sized. The

hyphae of the *dam1* $\Delta$  strain often changed direction leading to zigzag (or curved) morphology deviating from the rather straight trajectory followed by WT hyphae (Fig. 4.11D). I also looked at vegetative growth from conidia. Once again *dam1* $\Delta$  showed more frequent branching. Further, the cell compartments of *dam1* $\Delta$  showed a reduced length and increased diameter, which was rather irregular compared to the constant diameter seen in the WT. Dam1 function is thus crucial for maintenance of uniform hyphal morphology and patterning, through prevention of excessive branching and irregular hyphal cell diameter and length.

Interestingly, during interphase, distinct spots of GFP-Dam1 localised to the growing tip of the hypha (Fig. 4.12A). These spots were intense, highly dynamic, and appeared to track the growing tip (Fig. 4.12B). To study whether this non-canonical interphase localisation was restricted to Dam1 or involved other components of the DASH complex, I monitored the localisation of Ask1-GFP. Ask1-GFP localised to the growing tips of hyphae in a pattern reminiscent of Dam1 (Fig. 4.12C). Thus, distinct from their kinetochore function, during interphase dynamic DASH complex punctae migrate to hyphal tips under polarised growth.

Most MTs in the *A. nidulans* hyphal tips have their plus-ends oriented towards the direction of growth (Konzack et al., 2005). Motor proteins like kinesin KipA track along microtubules to the hyphal tip and collect at the MT plus-ends. Loss of KipA function alters MT-cortex interaction affecting maintenance of polarity during hyphal growth (Konzack et al., 2005). In view of the known plus-end MT binding of DASH complex subunits, MT plus end binding Dam1 likely contributes to the signal at the hyphal tip in *M. oryzae*, supporting apical growth. The sub-cellular localisation of *M. oryzae* Dam1 and Ask1 is akin to that of kinesin KipA and microtubule polymerase AlpA in *A. nidulans*.

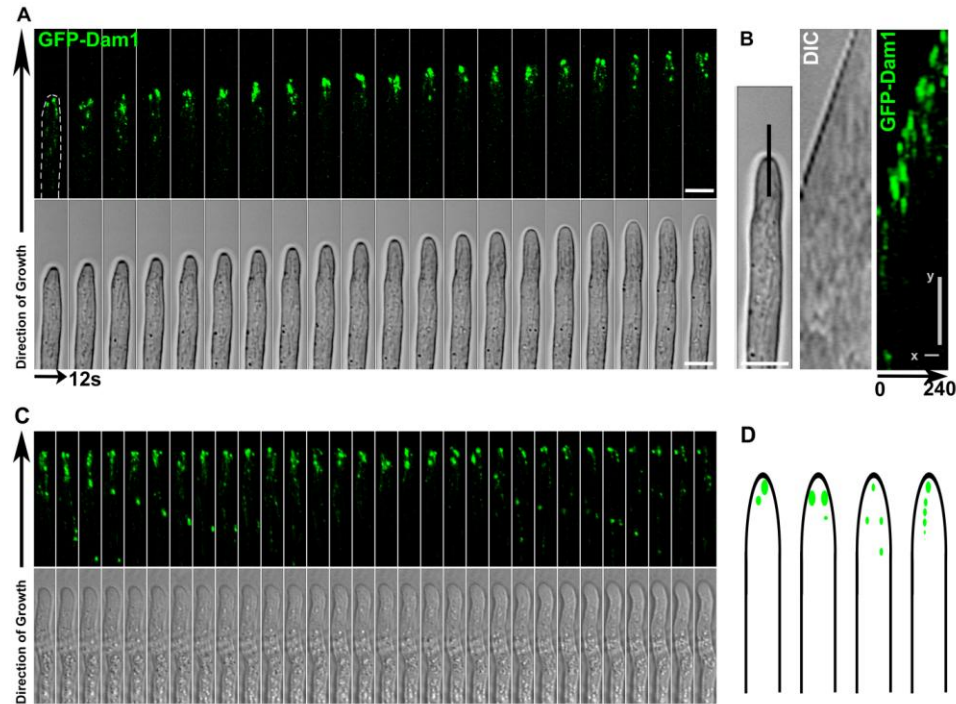


**Figure 4.12: DASH complex proteins Dam1 and Ask1 localise to the growing tip of the hypha**

A) Localisation of GFP–Dam1 at the hyphal tip during vegetative growth,  $n=30$ . Hyphal borders are shown with dashed lines. Scale bar = 5  $\mu\text{m}$ . B) Kymograph of time-lapse images of GFP–Dam1 shown in A. Kymograph is plotted along the black line marked on the hyphal tip in the left-hand panel for 240 s. Scale bars:  $x=48$  s,  $y=1.5$   $\mu\text{m}$ . C) Localisation of Ask1–GFP at the hyphal tip during vegetative growth. Scale bar = 5  $\mu\text{m}$ . D) Schematic depicting the GFP–Dam1 localisation patterns observed at the hyphal tip.

DASH complex punctae track cytoplasmic MTs (cMTs) in *S. pombe*, merging into larger oligomers from time to time, or crossing over to neighbouring MTs (Gao et al., 2010). Importantly, Dam1 alters the rate of spindle as well as cytoplasmic MT depolymerisation. Many of the facts discussed above provide strong support for the cytoplasmic microtubule association of *M. oryzae* Dam1 during interphase. While I have not captured GFP–Dam1 spots merging, I did observe spots of varying sizes. I suspect that the intense larger spots are those associated with the end of microtubules, while those migrating along the microtubules were smaller

in size. Further, it is possible that smaller oligomers travelling towards the tip merge into larger complexes at the tips. In *S. pombe* too, lateral as well as end-binding has been seen in case of Dam1-MT association.

The elongation of the germ tube from the conidium during early pathogenic development of *M. oryzae* relies on polarised growth. Dynamic Ask1-GFP and GFP-Dam1 punctae, were seen at the tips of germ tubes, similar to those seen in vegetative hyphae, suggesting a role for the DASH complex even during polarised pathogenic growth (Fig. 4.14A).

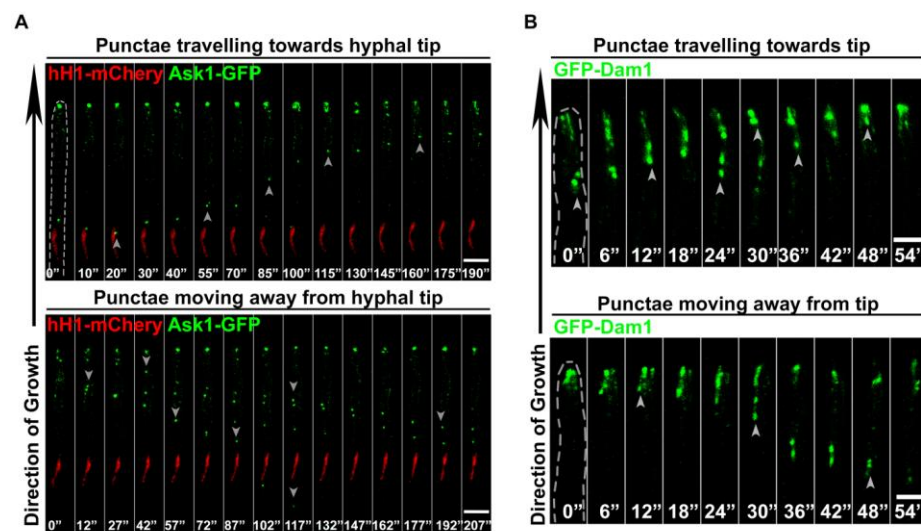


**Figure 4.13: Oscillation of DASH complex proteins**

A) Oscillation of Ask1-GFP from vegetative hyphal tip during interphase,  $n=20$ . Numbers indicate time in seconds. Hypha is outlined with dashed lines. Arrowheads mark the Ask1-GFP punctae moving towards or away from the tip. Scale bar = 5  $\mu\text{m}$ . B) Back-and-forth movement of GFP-Dam1 towards vegetative hyphal tip,  $n=10$ . Numbers indicate time in seconds. Hyphae are outlined with dashed lines. Arrowheads mark the GFP-Dam1 punctae moving towards or away from the tip. Scale bar = 3  $\mu\text{m}$ .

Intriguingly Ask1-GFP (Fig. 4.13A) and GFP-Dam1 (Fig. 4.13B) spots moved to and fro from the tip back towards the nucleus, indicating long distance migration along microtubule tracks. Further several different spots were seen simultaneously, migrating at different rates. The rate of

movement did not remain constant for a given puncta throughout its journey (Fig. 4.13A).

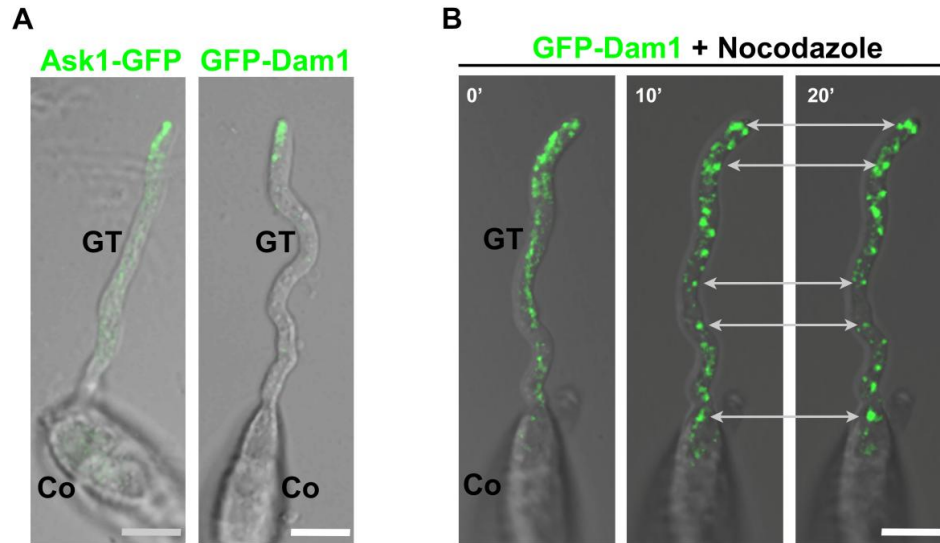


**Figure 4.14: Dam1 localises to the tip during polarised pathogenic development**

A) Ask1-GFP and GFP-Dam1 localise in the form of dynamic punctae to the germ tube tip during polarised growth under pathogenic development on a hydrophobic surface,  $n=25$ . Arrowheads mark Ask1-GFP or GFP-Dam1 at the germ tube tip. Scale bar = 10  $\mu\text{m}$ . B) Effect of nocodazole treatment on GFP-Dam1 localisation,  $n=20$ . Arrows mark the static large aggregates of GFP-Dam1 all along the germ tube post-nocodazole treatment. Scale bar = 5  $\mu\text{m}$ .

I inquired whether the oscillation of the DASH complex proteins during polarised growth relied on an intact microtubule network. On treating germinating conidia with nocodazole (a microtubule-destabilising agent), the GFP-Dam1 punctae lost their dynamic movement, forming cytoplasmic aggregates randomly distributed along the germ tube, suggesting that the MT network indeed guides DASH complex dynamics (Fig.4.14B).

Thus, the growth defects of the *dam1* $\Delta$  strain likely result from a combination of loss of Dam1 function at mitosis alongwith loss of cell

polarity during interphase cell growth. Long distance MT-based back and forth movement of Dam1 suggests a non-conventional function of the DASH complex protein during interphase in *Magnaporthe*.

It will be worth studying if the complex migrates to the tip as a whole or whether the complex is assembled at the tip itself. The dynamic oscillatory behaviour of GFP-Dam1 punctae along the hyphae is altered in the absence of Ask1, showing fewer slow-moving punctae, supporting the possibility that Dam1 and Ask1 proteins may migrate to the tip as a complex. A strain with more than one DASH complex subunit tagged simultaneously would provide a better understanding of the association of these proteins during interphase. Further, studying interactions, if any, between the *M. oryzae* Dam1 and other microtubule-associated proteins and motor proteins, and their role in regulating the MT network, particularly during interphase that occupies a large part of the *M. oryzae* cell cycle may provide interesting findings specific to filamentous fungi.

#### **4.5 Conidiation (or sporulation) in *M. oryzae* is dependent on Dam1**

Alongwith reduced colony diameter, the *dam1* $\Delta$  strain only develops flat, weakly melanised growth, in stark contrast to the fluffy, dark grey colonies of the WT. Such growth patterns arise from impaired growth of aerial hyphae that bear conidia, making it worth investigating Dam1 function in conidiation.

The formation of spores and their morphology have been an important criterion in identification and classification of fungi. Conidia are asexual spores produced by mitosis. Though *M. oryzae* also produce crescent-shaped unicellular asexual microconidia, they have only been isolated under certain specific growth conditions and have not been observed on diseased plants in the field so far. The three-celled pyriform macroconidia are responsible for the widespread infections and for simplicity are referred to as conidia throughout this study. The development of three celled conidia is crucial for initiation of a new cycle of *M. oryzae* infection.

One of the reasons for the severity of rice blast infections is the ability of *M. oryzae* to complete many disease cycles within a given cropping season under favourable climatic conditions. The spread of the disease to new plants relies on the production of asexual conidia which emerge from infected plant tissues within 3–5 days, and continue to develop as the lesions spread across the leaf tissue. Investigating the molecular mechanisms of conidium development will enable the development of strategies for preventing the spread of the disease and its restriction to infected hosts. Conidiation has previously been characterised in *A. nidulans* and *N. crassa*, however the conidium structure and arrangement of conidia in these filamentous fungi is different from that in *M. oryzae*. Conidiation in *M. oryzae* is one of the lesser understood processes compared to the pre-infection appressorium development and *in planta* invasion, such that unlike the other stages of the *M. oryzae* infection cycle, the details of the cell cycle and the process of mitosis involved in conidiation have not been studied in detail.

Conidiogenesis in *M. oryzae* takes place on specialised aerial hyphae called conidiophores. Humidity and light exposure positively affect the efficiency of conidiation, and contact with aerial environment is necessary for conidiation. *M. oryzae* asexual conidia (spores) are arranged sympodially, in clusters of three or more, at the tip of the conidiophore (Howard 1994). The conidiophore tip swells in a switch from polarised to isotropic growth to form the first conidium of the bunch. The apical tip of the conidiophores then bends away to the other side to form the next conidium. This continues till a cluster is formed, sometimes forming even up to 7-8 conidia per stalk, but commonly clusters range between 3-5 conidia. Thus, the sympodial arrangement of conidiophores relies on the ability of the conidiophore cell to undergo multiple cell divisions, each time providing a nucleus to the new incipient conidium through a fresh round of mitosis.

## 4.5.1 Dam1 function is crucial for proper conidiation

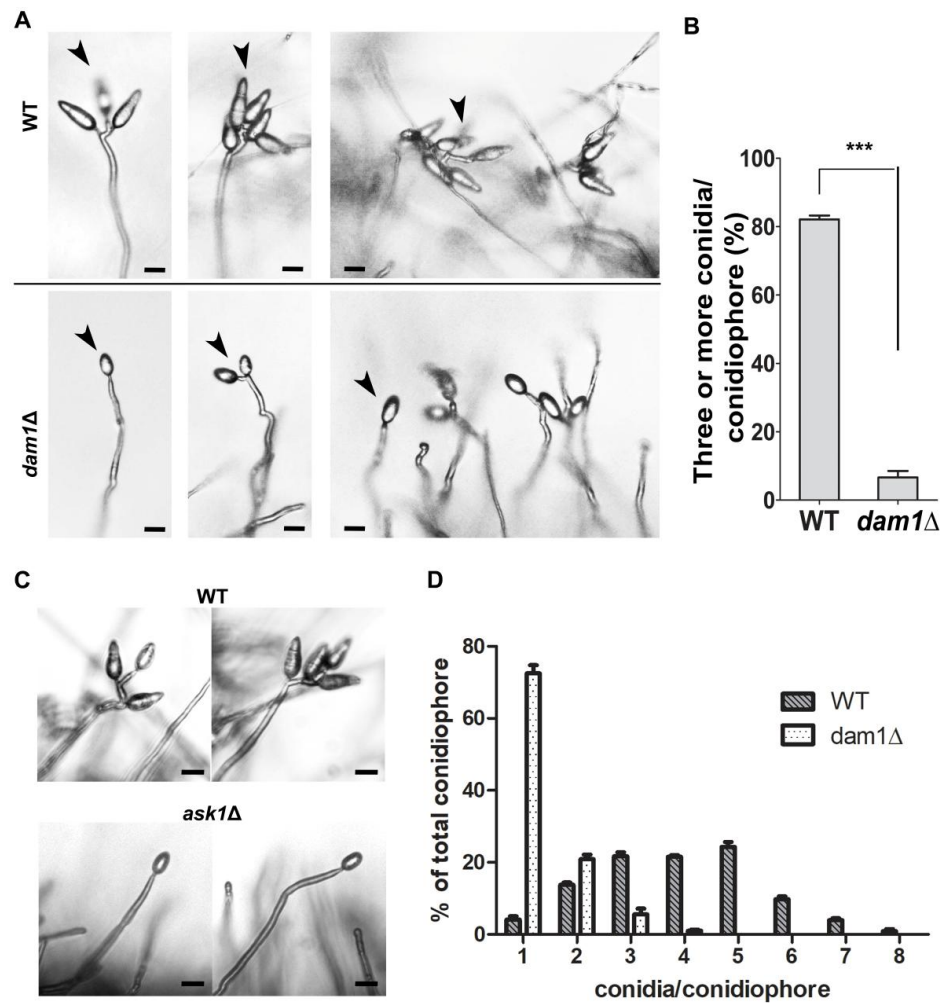


**Figure 4.15: Loss of Dam1 function significantly alters conidiation**

A) Difference between the WT and *dam1Δ* in the number of sympodial conidia borne per conidiophore (arrowheads). Scale bar = 10  $\mu$ m. B) Bar chart showing mean  $\pm$  S.E.M. frequency of conidiophores bearing three or more conidia in the *dam1Δ* compared to the WT strain. \*\*\* $P < 0.0001$ , two-tailed *t*-test,  $n = 300$  conidiophores. C) Difference in the conidium arrangement on conidiophore between WT and *ask1Δ*. Scale bar = 10  $\mu$ m. D) Bar chart showing distribution of conidiophores in WT and *dam1Δ* strains.

To assess the role of the Dam1 protein during development of asexual conidia, I observed the organisation and morphology of conidiophores. The WT strain produced sympodial clusters of 3 to 5 conidia after 24hrs of

photo-induction (Fig. 4.15A, B). However, most of the *dam1Δ* conidiophores bore only 1 to 3 conidia. Total conidiation in the *dam1Δ* strain was reduced to one-tenth of WT counts indicating a decline in overall conidiation efficiency (N = 3, P<0.001, two-tailed *t* test).

In *Magnaporthe* several genetic mutations have an impact on conidiation or sporulation efficiency without affecting the morphology or three-cell structure, as listed in Table 1. While mutations that increase sporulation efficiency have been discovered, the number is low and most mutations negatively impact sporulation. Decreased conidiation is often found to be a consequence of fewer aerial hyphae and conidiophores (Table 4.1).

**Table 4.1: Genes/ Proteins involved in conidiation in *M. oryzae***

Gene/ Locus/ Protein	Conidiation/ Sporulation	Morphology	Reference
Con1	Reduced by 90%	Elongated- twice as long and half as wide	(Shi and Leung, 1994, Shi and Leung, 1995)
Con2	Reduced by 90%	Aconidial in dark, Misshapen- 1- or 2- celled conidia in light	(Shi and Leung, 1994, Shi and Leung, 1995)
Con4	Reduced by 35%	Abnormal morphology	(Shi and Leung, 1994, Shi and Leung, 1995)
Con5	Abolished	Conidiophore formation blocked	(Shi and Leung, 1995)
Con6	Abolished	Abundant conidiophores formed, no conidia	(Shi and Leung, 1995)
Con7 Transcription factor	Reduced by 35%	Heterogenous, Abnormal morphology- basal protruberance, reduced number of septa	Shi and Leung 1995, Shi et al 1998, (Odenbach et al., 2007)
Adenylate cyclase MAC1	Reduced	-	(Choi and Dean, 1997)
MedA homolog ACR1 (acropetal)	-	Altered spore arrangement and morphology-chain of spores, altered number of septa	(Lau and Hamer, 1998) Nishimura et al.,2000)
Protein kinase MPS1	Reduced	Reduced aerial hyphae	(Xu et al., 1998)
Blue light receptor MgWC1	Delayed, Spore release affected	-	(Lee et al., 2006)
Trehalose-6-	Reduced	-	(Wilson et al.,

phosphate synthase Tps1			2007)
Rgs1	Increased sporulation	-	(Liu et al., 2007)
Mgb1, a G protein B subunit MagB	Reduced	Reduced aerial hyphae and conidiophores	(Liu et al., 2007)
Mads box protein MIG1	Reduced	Reduced aerial hyphae	(Mehrabi et al., 2008)
Rho family GTPase MgRac1	Reduced three orders of magnitude	abnormal elongated morphology, with basal appendage	(Chen et al., 2008)
Putative MAP kinase kinase kinase MCK1	Reduced to 5%	Fewer conidiophores, single conidium per conidiophore	(Jeon et al., 2008)
<i>MTP1</i> (Type III integral transmembrane protein, similar to yeast Ytp1)	Reduced	-	(Lu et al., 2008)
Protein kinase MoSNF1	Reduced	Few conidiophores, One or two per conidia, Abnormal shape, 1-, 2- or 4-cell conidia	(Yi et al., 2008)
Zn finger transcription factor, Cos1	Abolished	No Conidiophore development	Zhou et al., 2009
MStu1 APSES transcription factor	Reduced	-	Nishimura et al 2009
Lhs1 Hsp70 family	Reduced 0.3-4%	Reduced conidiophore formation, 1 or 2 conidia per conidiophore	(Yi et al., 2009)
MoAtg8	Reduced to ~2%	Reduced conidiophore differentiation, Lower conidium viability	(Deng et al., 2009)
Calcineurin responsive transcription factor MoCrz1	Reduced to 15%	-	(Choi et al., 2009)
SMO	No change	Abnormal morphology	(Hamer et al., 1989; Kershaw et al., 2019) Kershaw et al., 2019
MoHox2 transcription factor / HTF1		Conidium and conidiophore formation	Kim et al.,2009; Liu et al.,2010
Snare homolog MoSec22	Fail to produce conidia	No conidiophores	Song et al., 2010
Tea4	Reduced to less than 1%	Mostly 80% 2-celled conidia with single septum	(Patkar et al., 2010)
PdeH, a high-affinity cAMP phosphodiesterase,	Increased	Conidiophore higher, more conidia per conidiophore	(Ramanujam and Naqvi, 2010)
Transcription regulator Com1	-	Altered morphology-Thin and long conidia with	(Yang et al., 2010)

		wide basal appendage, smaller and fewer lipid droplets	
Sterol 14alpha-demethylase CYP51A	Reduced	-	(Yan et al., 2011b)
Cell cycle gene Cdc15	Reduced	Fewer conidiophores, 1 or 2 conidia per conidiophore, abnormal shape and septation defects, 2, 4 or 5 celled conidia	(Goh et al., 2011)
MADS-box transcription factor MoMcm1	Reduced	Reduced aerial hyphae	(Zhou et al., 2011)
Transcriptional regulators MoSom1, MoCdtf1	Abolished	-	(Yan et al., 2011a)
Phospholipase C MoPlc2 and MoPlc3	Reduced	-	(Choi et al., 2011)
Sorting nexin Snx41	Loss of conidiation	-	(Deng et al., 2012)
MoTsc13	-	Abnormal morphology-two celled conidia	(He et al., 2012)
MoMon1	Reduced to 0.5%	Aerial hyphae reduced, abnormal conidium morphology	(Gao et al., 2013)
Serine/ threonine-protein phosphatase PP2A	Reduced to 0.1%	80% two-cell with septum, rest 1-cell conidia	(Du et al., 2013)
Atg24	Reduced to less than 1%	Reduced conidiophores	(He et al., 2013)
Pac2 family transcriptional regulator MoGti1	Reduced to 5%	-	(Chen et al., 2014a)
Pac2 family transcriptional regulator MoPac1	Increased twofold	-	(Chen et al., 2014a)
MoLys2 (Lysine biosynthesis)	No conidiation, restored by supplementation	-	(Chen et al., 2014b)
Threonine deaminase MoILV1	Reduced	Conidiophores reduced, 1-, 2- and 3-cell conidia	(Du et al., 2014)
MoST1 encoding a hexose transporter-like protein	50 times less	-	(Saitoh et al., 2014)
RhoGAP proteins	Reduced	Abnormal morphology, Reduced aerial hyphae, reduced septa, few conidia per conidiophore	(Ye et al., 2014)
Num1 ortholog	Reduced to	Heterogenous	(Jeon et al., 2014)

MoAnd1	35% of WT	morphology based on size and septation	
APSES transcription factors MoAps1 and MoAps2	Reduced	-	(Park et al., 2013)
MoTup1	Reduced to less than 1%	-	(Chen et al., 2015)
MoGrr1, F-box protein	Abolished	No conidiophores	(Guo et al., 2015)
Mitochondrial fission protein MoFis1	Reduced	Fewer conidiophores	(Khan et al., 2015)
Gamma subunit gene MGG1	Reduced to 10%	-	(Li et al., 2015)
MoARG1, MoARG5, 6 and MoARG7 Arginine biosynthesis	Abolished, MoARG7-reduced	Restored by supplementation-morphologically defective 1- or 2-cell conidia	(Zhang et al., 2015a)
S-(hydroxymethyl) glutathione dehydrogenase	Reduced to 2%	-	(Zhang et al., 2015b)
MoMyb1	Abolished	-	(Dong et al., 2015)
Phosphotransferase MoYpd1/ MoHpt1	Reduced	-	(Jacob et al., 2015; Mohanan et al., 2017)
MoCDC14	Reduced more than 100 fold	Aberrant, 99% were 1-celled, incomplete septation, 1 or 2 nuclei	(Li et al., 2016a)
Skp1, a component of E3 ubiquitin ligase	Reduced	-	(Prakash et al., 2016)
Magnesium transporter Alr1	Failure to sporulate	-	(Reza et al., 2016)
Magnesium transporter Mnr2	Reduced	-	(Reza et al., 2016)
Syntaxin protein (MoSyn8)	Reduced	Some abnormal with one septum, narrow morphology	(Qi et al., 2016)
Glycoside Hydrolase MoGls2	Increased 1.5 times	-	(Li et al., 2016b)
Calpains, Capn7	1/70 <sup>th</sup> of the WT	-	(Liu et al., 2016)
Arf6	Reduced	Abnormal misshapen morphology, 1- or 2-cell conidia	(Zhu et al., 2016)
Electron transfer flavoproteins ETFA and ETFB	Reduced to 8-10%	-	(Li et al., 2016c)
MoCps1	Reduced	Altered morphology	(Wang et al., 2016)
MoYcp4	Increased 10 fold	-	(Chen et al., 2017)
Class-II myosin	Reduced	Conidiophore reduced, morphology abnormal	(Guo et al., 2017)
WD40-repeat	Reduced to	Reduced conidiophores,	(Matar et al., 2017)

protein MoCreC	25%	Smaller, 60% 1- or 2-celled	
Methylmalonate-semialdehyde dehydrogenase	Reduced	Conidiophore reduced	(Norvinyeku et al., 2017)
BAS1 overexpression	Increased	-	(Yang et al., 2017)
Glutamate synthase MoGlt1	Reduced to less than 10%	Fewer conidiophores, conidiophore with 1 or 2 conidia	(Zhou et al., 2017)
Atypical Guanylate Kinase MoGuk2	Reduced by 87%	53% with abnormal morphology, one or two septa	(Cai et al., 2017)
Movrp1 Putative Verpolin protein	Abolished	-	(Huang et al., 2017)
WISH, a novel CFEM GPCR	Increased	Enhanced conidiophore formation	(Sabnam and Roy Barman, 2017)
FLB3 and FLB4	Reduced	aberrant morphology	(Matheis et al., 2017)
Sumoylation genes MoSmt3, Moaos1, Mouba2, MoUbc9	Reduced to ~10%	One or two conidia per conidiophore	(Lim et al., 2018)
Zn finger –like metal binding domain MoYPEL1	Reduced by 22%	-	(Han et al., 2018)
Zn finger –like metal binding domain MoYPEL2	Increased by 151%	-	(Han et al., 2018)
MoIVD-Mediated Leucine Catabolism	Reduced to 2/3 of WT	Fewer conidiophores	(Li et al., 2019)

Further, the *dam1Δ* mutant, when stained with CFW, showed aberrant conidium morphology. In contrast to the three-cell pyriform WT-like conidia, *dam1Δ* predominantly developed oval one- or two-cell conidia (Fig. 4.16A, B). The mutant conidia were also shorter (14 μm) than the WT (23 μm) (Fig. 4.16D). Interestingly, though majority of the conidia were single celled based on CFW staining, they had attained an average length of two-celled conidia. It is likely that many conidia have been arrested or collapsed due to improper segregation during the mitotic event.

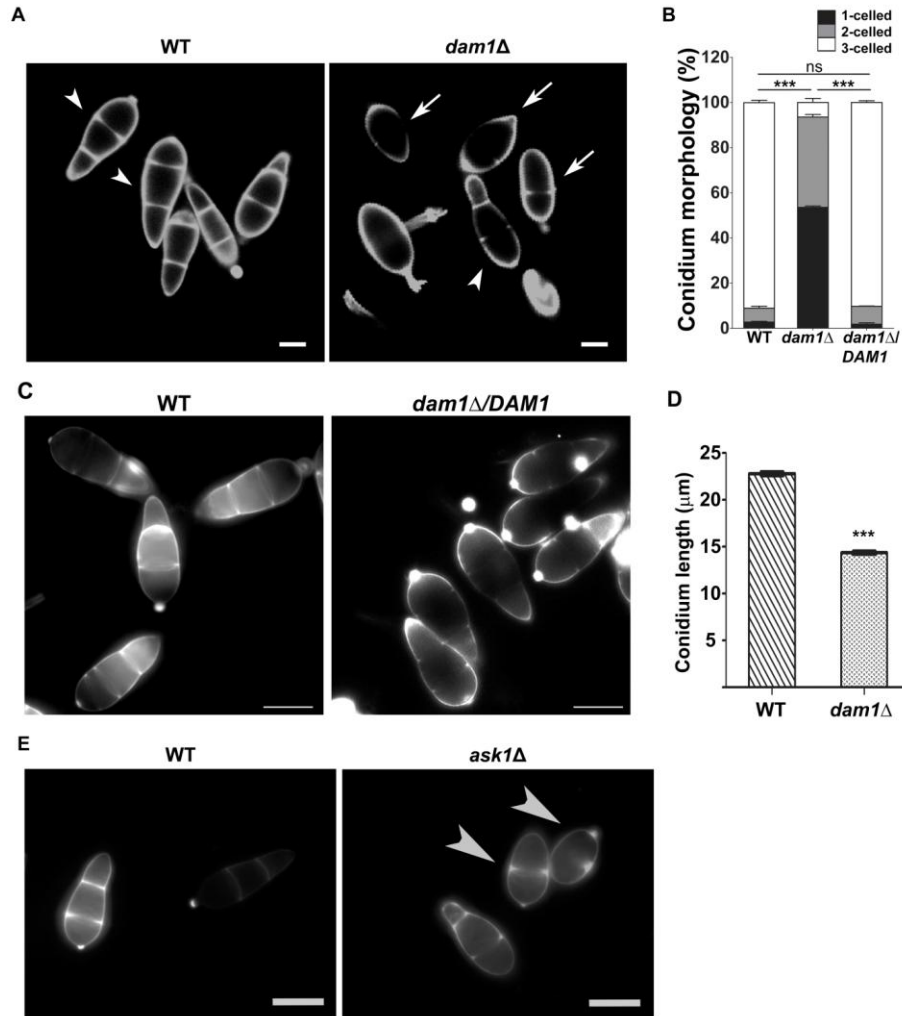


**Figure 4.16: DASH complex proteins play a role in conidium morphology**

A) Morphology of WT and *dam1Δ* conidia stained with CFW. Arrowheads depict 3-celled conidia and arrows indicate 1- or 2-celled conidia. Scale bar = 5 μm. B) Bar chart showing mean ± S.E.M. frequency of conidia with different cell numbers (1, 2 or 3) in the WT, *dam1Δ* or *dam1Δ/DAM1* strain. \*\*\* $P < 0.0001$ ; ns, not significantly different; two-tailed *t*-test,  $n = 300$ . C) Morphology of WT and *dam1Δ/DAM1* conidia stained with CFW. Scale bar = 10 μm. D) Bar chart showing mean ± S.E.M. length of conidia in the WT and *dam1Δ* strain. \*\*\* $P < 0.0001$ ; two-tailed *t*-test,  $n = 300$ . E) Morphology of WT and *ask1Δ* conidia stained with CFW. Arrowheads depict 1- or 2-celled conidia. Scale bar = 10 μm.

Further, since the pyriform shape is achieved during growth and formation of the third conidial cell, and many conidia did not proceed to this stage, most of the conidia showed the oval morphology, with an altered

width:length ratio compared to the WT. The conidial morphology was restored to wild-type in the complementation strain *dam1Δ/DAMI* (Fig. 4.16C). The *ask1Δ* mutant was also impaired in conidiation efficiency and morphology (Fig. 4.16E). Occasionally, there were also incomplete septa or irregular chitin deposition seen within the conidia (Fig. 4.16E).

As highlighted (in blue) in Table 1, fewer studies describe genes affecting conidium morphology and arrangement. Earlier, mutagenesis-based screens identified several loci affecting conidial morphology and arrangement. For example, mutations at the SMO locus (spore morphology), *smo1-1* and *smo1-3*, produce a variety of 1- or 2-cell spherical or misshapen conidia. However, conidiation efficiency is unaffected in *smo* mutants (Hamer et al., 1989). *SMO1* was characterised very recently and codes for a Ras GTPase activating protein (Kershaw et al., 2019). Disruption of the *ACR1* gene produces a chain of head-to-tail arranged conidia instead of the sympodial conidiophore (Lau and Hamer, 1998; Nishimura et al., 2000). Random chemical and insertional mutagenesis uncovered several other loci affecting conidiation, referred to as CON mutants, but most of these loci have not been characterised (Shi and Leung, 1995; Shi et al., 1998). *con5* and *con6* mutants do not sporulate, *con1* and *con2* strains display reduced conidiation and produce abnormal conidia, and *con4* and *con7* mutants have abnormal morphology but do not affect conidium production. Con7 is a zinc-finger transcription factor that regulates genes involved in cell wall biogenesis (Odenbach et al., 2007). COS1 and MoHox2 are two other transcription factors that affect conidiophore development and conidium formation. Several genes induced during conidiation are regulated by MoHox2 (Kim et al., 2009; Liu et al., 2010). FLB3 and FLB4 mutants can be classified into several categories as was seen with the *con* mutants, indicating that several different factors and pathways function to achieve the sympodially arranged three-cell conidia. Conidiation was reduced three fold in MgRac1 (Rho family GTPase) deletion mutants, and the few conidia that were

produced showed an abnormal elongated morphology with a basal appendage, likely due to improper detachment. Thus, a small proportion of genes affecting conidiation show changes in conidium morphology-shape (length/width) or cell number and even in the aberrant morphology there is a great deal of heterogeneity between different genes. However, most of these morphologies are different from those seen in *dam1Δ*.

The genes that showed defects closest to *dam1Δ* included MoDuo1, a DASH complex member previously implicated in proper conidiation (Peng et al., 2011). Other genes with similar mutant phenotypes included the polarity factors *MoTEA4*, and *MoSPA2* and the nuclear positioning gene *MoAND1*. Loss of Tea4 function, which is important for maintenance of cell polarity in *M. oryzae*, led to defective septation, similar to that in the *dam1Δ* conidia, producing oval 1- or 2- cell conidia (Patkar et al., 2010). Though the proportion of 1-cell conidia is much higher in absence of Dam1, it is likely that Dam1 and Tea4 are involved in a common process during polarised growth, and the difference in severity of defect may be due to the specific role of Dam1 protein during mitosis. *MoAND1* deletion has shown that nuclear positioning is a key factor in conidium development (Jeon et al., 2014). Earlier I have shown in appressoria and vegetative hyphae, that Dam1 persists for a while after mitosis during nuclear migration, until the nucleus reaches the appropriate site. Since *dam1Δ* show similar phenotypes, it is likely that Dam1 may also play a role in nuclear positioning after mitosis.

WT conidia show distinct cell boundaries between the three cells. Each cell shows one nucleus and a microtubule network distributed all over the cell. An intense network is seen at the septa, likely emerging from septal MTOCs (Fig. 4.17A, C).

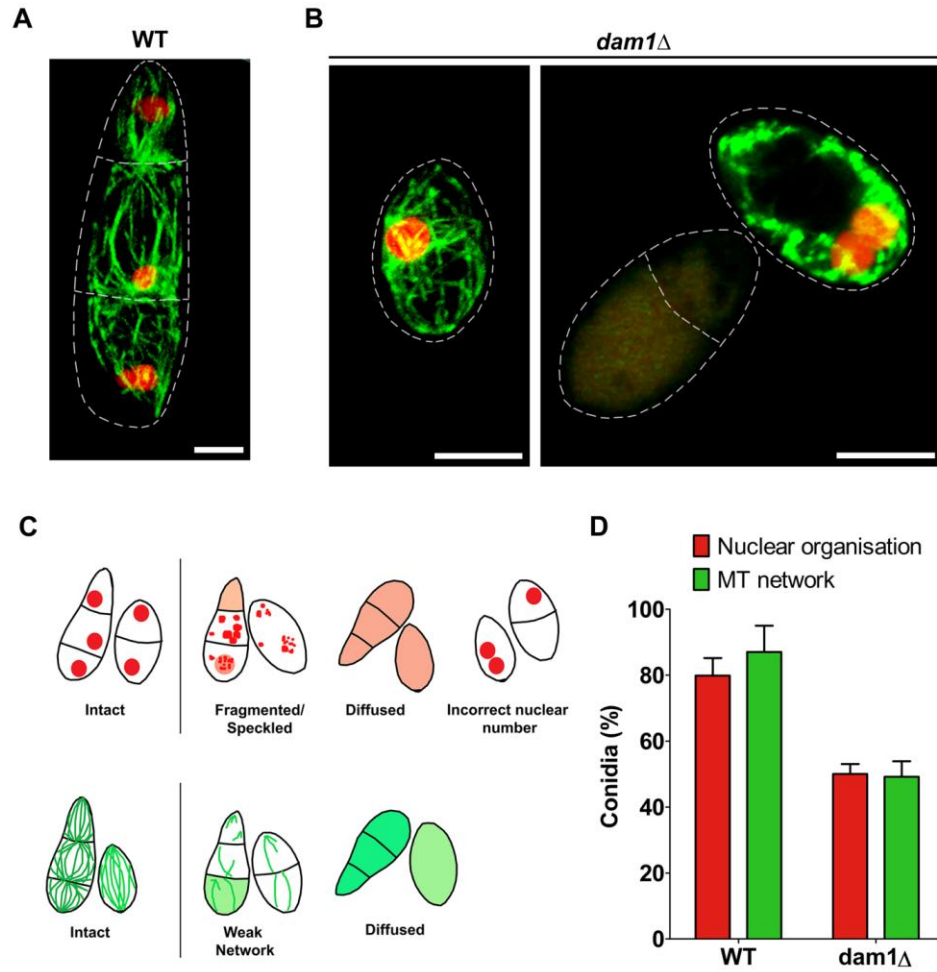


**Figure 4.17: Nuclear organisation and microtubule network in conidia is affected by loss of Dam1**

A) Nuclear organization and MT network in WT conidia expressing hH1-mCherry and Tub-GFP. Conidia borders are shown with dashed lines. Scale bar = 5  $\mu$ m. B) *dam1Δ* conidia C) Schematic showing the different types of nuclear structure and MT network observed in conidia of WT and *dam1Δ* strains. D) Bar chart showing mean  $\pm$  S.E.M. number of conidia with intact nuclear and MT organization in the WT and *dam1Δ* mutant strains from three independent experiments. \*\* $P < 0.05$ , two-tailed t-test,  $n = 100$ . Data represents mean  $\pm$  S.E.M. from three independent experiments.

About half the *dam1Δ* conidial population lacked the standard nuclear and microtubular structures, often showing diffused cytoplasmic signal (Fig. 4.17B, D). Further, around 30% of the *dam1Δ* conidia showed defects in

nuclear morphology as well as MT network, likely contributing to the lack of conidium viability. In summary, conidial development was significantly impaired in the absence of Dam1 function mostly due to an atypical microtubule network structure and/or unequal nuclear segregation resulting in aberrant septation and cell number. To investigate further I studied the localisation of Dam1 during three rounds of mitosis during conidial development.

#### **4.5.1 Conidium development displays a convergence of distinct cell division patterns**

*Magnaporthe* undergoes holoblastic conidiogenesis where the conidial cell bulges out from the conidiophore and is delineated by a septum similar to the process of budding in yeasts. Differentiation of the germ tube to form the dome-shaped appressorium and the conidiophore into conidium follow an analogous morphogenetic switch from polarised to isotropic growth accompanied by an asymmetric cell division. While the role of cell cycle-based regulation of appressorial development is established. Such studies describing conidiophore development have proved to be technically more challenging in *Magnaporthe* and are scarce.

In this study, I monitored the process of mitosis during the development of the conidium in the strain with the fluorescently labelled nucleus and microtubules. Development of the three-cell conidium on an average takes 5-7 hours, with rapid mitosis spanning a few minutes, separated by 1.5-2.5 hr interphases characterised by cell growth and changes in cell shape. Conidium development is initiated by transitioning from polarised extension to isotropic expansion of the tip of the aerial hypha to give rise to the conidiophore on which the incipient conidium is borne (Deng et al., 2009). The first mitosis event occurred in the stalk (mitosis I; Fig. 4.18A). Subsequently, one daughter nucleus migrated to the conidium cell and the other stayed in the stalk to allow development of another sympodial

conidium. This was followed by cytokinesis (septation), which most likely occurred at the base of the conidium, distant from the position of the mitosis event in the stalk. Two distinct septation patterns have been described in *M. oryzae* based on the site of septation in relation to site of mitosis– 1) septation at the site of mitosis in growing hyphae (spatial coupling), and 2) cytokinesis spatially unlinked from mitosis during appressorium formation, wherein the septum is laid at the neck of the appressorium far away from the site of mitosis in the germ tube (Saunders et al., 2010). The spatial uncoupling of cytokinesis from the site of mitosis I during conidiation was reminiscent of the uncoupling observed during appressorium development, and different from tight association of nuclear and cell division in vegetative hyphae.

Elongation and enlargement of the single-celled spherical conidium follows cell division to form an oval cell, similar to the ones observed in the *dam1* $\Delta$  mutant, with the nucleus close to the centre of the sphere. This nucleus then undergoes mitosis-II, with one daughter nucleus shifted to the base (towards the stalk) of the conidium and the pushed towards the apex of the conidium. Mitosis was followed by cell division with septation at the site of mitosis to form an intermediate two-cell conidium, accompanied by corresponding changes in cellular microtubule organisation (mitosis II; Fig. 4.18A). Subsequently, the apical cell nucleus underwent the third round of division, and septation led to the formation of the mature pyriform 3-cell conidium (mitosis III; Fig 4.20). The deposition of the two subsequent septa in the developing conidium occurred at the site of mitosis as seen in the case of vegetative hyphae (Fig. 4.18A, B). Thus, I observed both the types of cytokinesis, previously described during two different developmental stages, converge during conidiation to form the aerial three celled conidium.

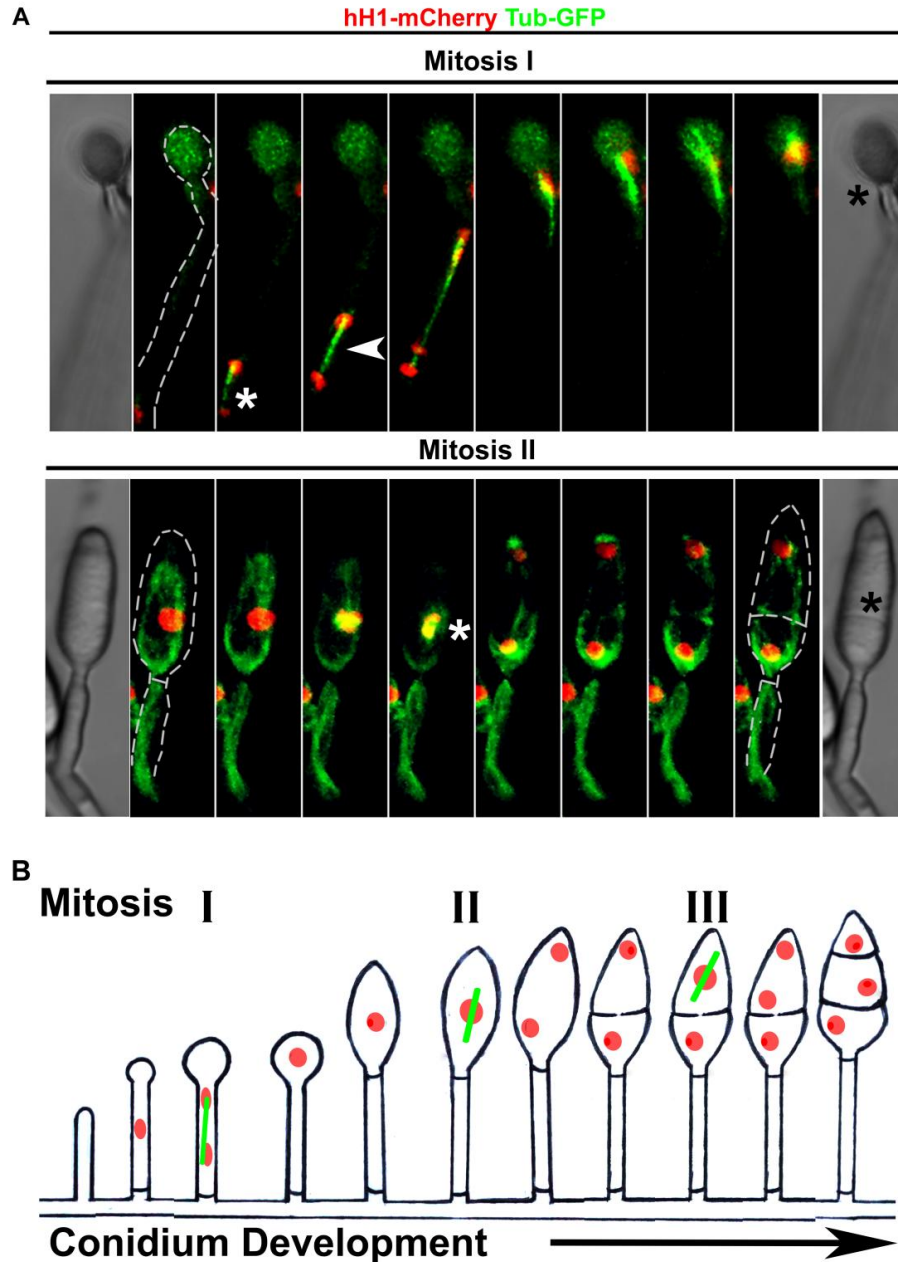


**Figure 4.18: Conidium development requires three distinct mitosis events**

Dynamics of Tub-GFP-marked MTs or spindle, and hH1-mCherry-marked nuclear division during mitosis in the developing conidium,  $n = 3$ . Mitosis I is observed in the stalk of the incipient conidium. Arrowheads mark the spindle, white asterisks indicate the site of mitosis, red asterisks denote the site of cytokinesis. Scale bar = 5  $\mu$ m. B) Schematic showing the different stages of conidium development.

Next, I used the information, about the morphological changes observed during conidiation and their correlation with the timing and site of mitosis, gained above to monitor the localisation patterns of Mis12-GFP and GFP-Dam1 during conidium development-associated mitosis events.

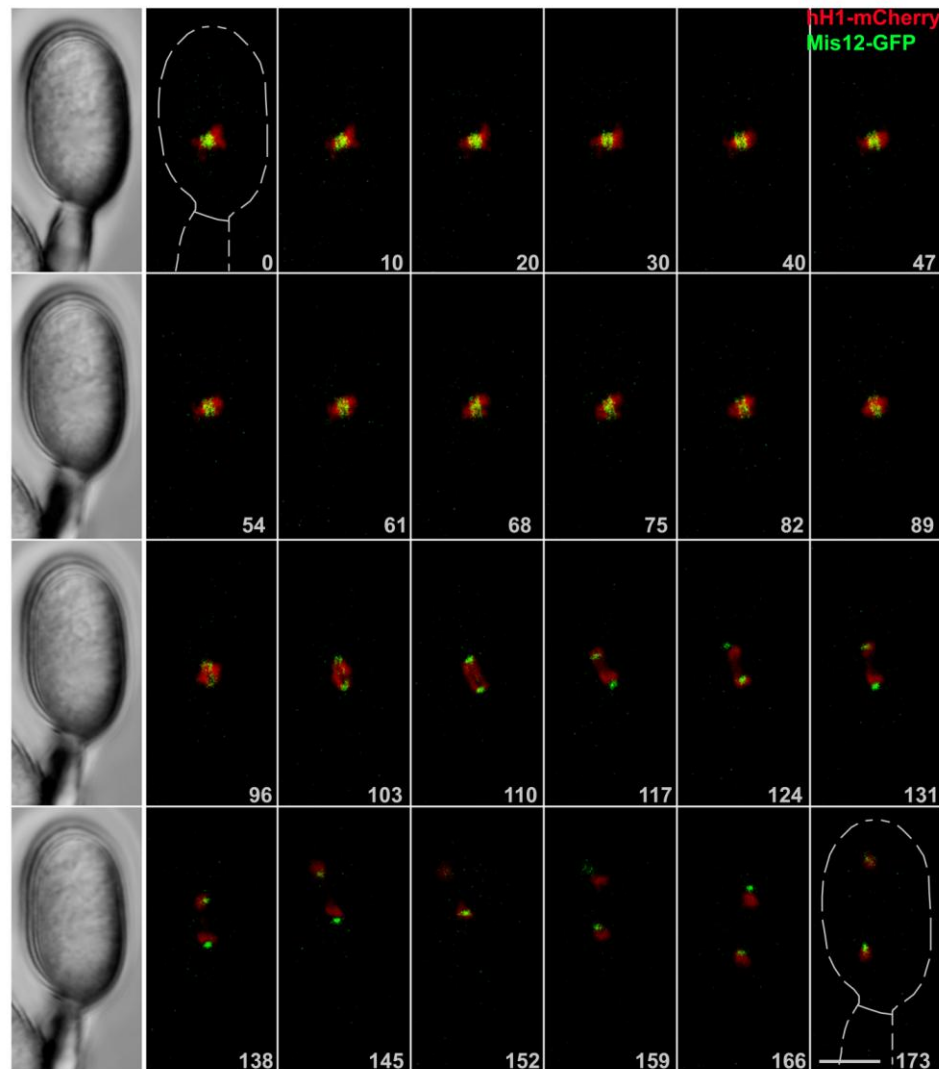


**Figure 4.19: Localisation of Mis12-GFP during mitosis II in the developing conidium**

Numbers indicate time in seconds. First column on the left depicts the DIC images corresponding to the panel of fluorescent images positioned right next them, namely timepoints 0, 54, 96 and 138. Conidium structures are shown with dashed grey outlines. Scale bar = 5  $\mu$ m.

As seen with vegetative hyphae and appressorium development, Mis12-GFP associated with the nucleus throughout the cell cycle during conidiation (Fig. 4.19). Even here, the Mis12-GFP cluster resolved into many individual foci associated with the chromosomes during mitosis and re-clustered into two distinct foci, one per nucleus, during anaphase. The duration of mitosis was quite similar to that observed in vegetative hyphae, on average ranging from 3-5 minutes.

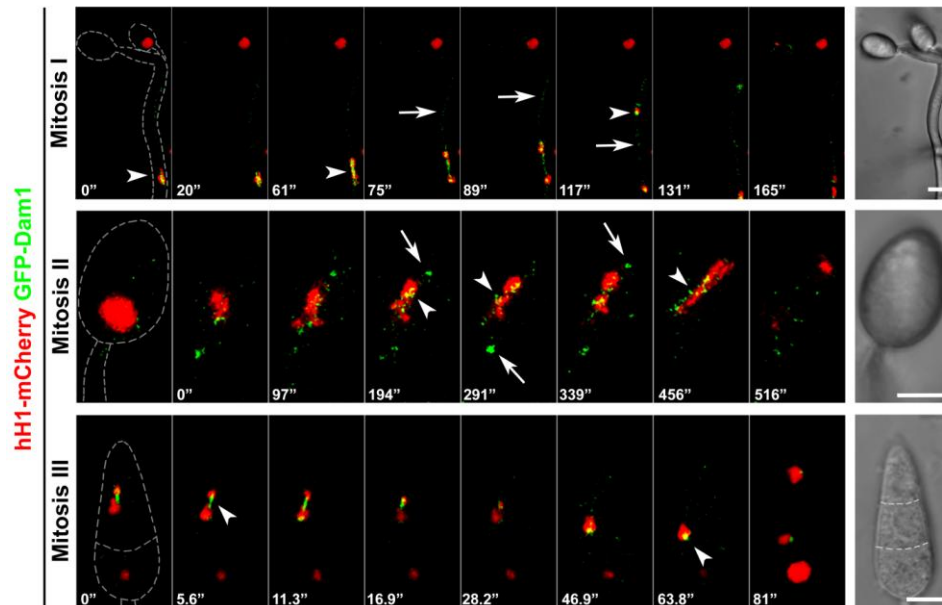


**Figure 4.20: Subcellular localisation of GFP-Dam1 during three mitoses in conidium development**

Localisation of GFP-Dam1 during three successive rounds of mitosis in the developing conidium,  $n=3$ . Numbers indicate time in seconds. Fungal structures are shown with dashed grey outlines. Arrowheads depict nuclear-associated GFP-Dam1, arrows indicate additional non-nuclear GFP-Dam1 spots. Scale bar = 5  $\mu\text{m}$ .

Subsequently, I investigated the sub-cellular pattern of GFP-Dam1 localisation in mitoses through conidial development. GFP-Dam1 associated with the nucleus during all 3 rounds of mitosis (Fig. 4.20). Several GFP-Dam1 spots were seen during mitosis that then coalesced into two distinct spots, one associated with each nucleus. The nuclear

association was maintained after anaphase till positioning of the nuclei was achieved.

Further during mitosis, several other cytoplasmic GFP-Dam1 spots, of varying intensity, were seen in addition to the nuclear-associated spots. The intense cytoplasmic spots were probably associated with the spindle pole body, while the weaker spots may have been associated with kintochore or astral microtubules. GFP-Dam1 or Ask1-GFP, as observed earlier in vegetative hyphae, lacked nuclear association during the intermittent interphases even during conidium development. Rarely, a cytoplasmic Dam1 spot was seen during the initial conidiophore bulging before the first nucleus had entered the cell. Thus, DASH complex function is important to the three consecutive rounds of mitosis and is indispensable to formation of WT-like asexual conidium. The sexual ascospores produced by *Magnaporthe* are 4-cell symmetric conidia and their formation also includes multiple rounds of nuclear division. It is likely that Dam1 is involved in the development of sexual spores as well and *dam1* $\Delta$  ascospores may have defective morphology, septation and cell number. Thus, proper development of asexual conidia in *M. oryzae* is likely dependent on the ability of Dam1 to bring about proper mitotic progression.

#### **4.6 DASH complex protein Dam1 is required for pathogenic development and virulence**

I studied appressorial (early pathogenic) development in the *dam1* $\Delta$  strain, to assess the role of Dam1 in the virulence of *M. oryzae*. In *in vitro* assays on hydrophobic coverglass, germination failed in most of the *dam1* $\Delta$  conidia (Fig. 4.21 A, B). This may be due to aberrant nuclear morphology and collapsed MT network in the conidia as shown earlier, leading to reduced conidial viability leading to an inability to germinate. Polarised germ tube extension is supported by an active MT network and altering MT dynamics would likely affect germ tube extension.

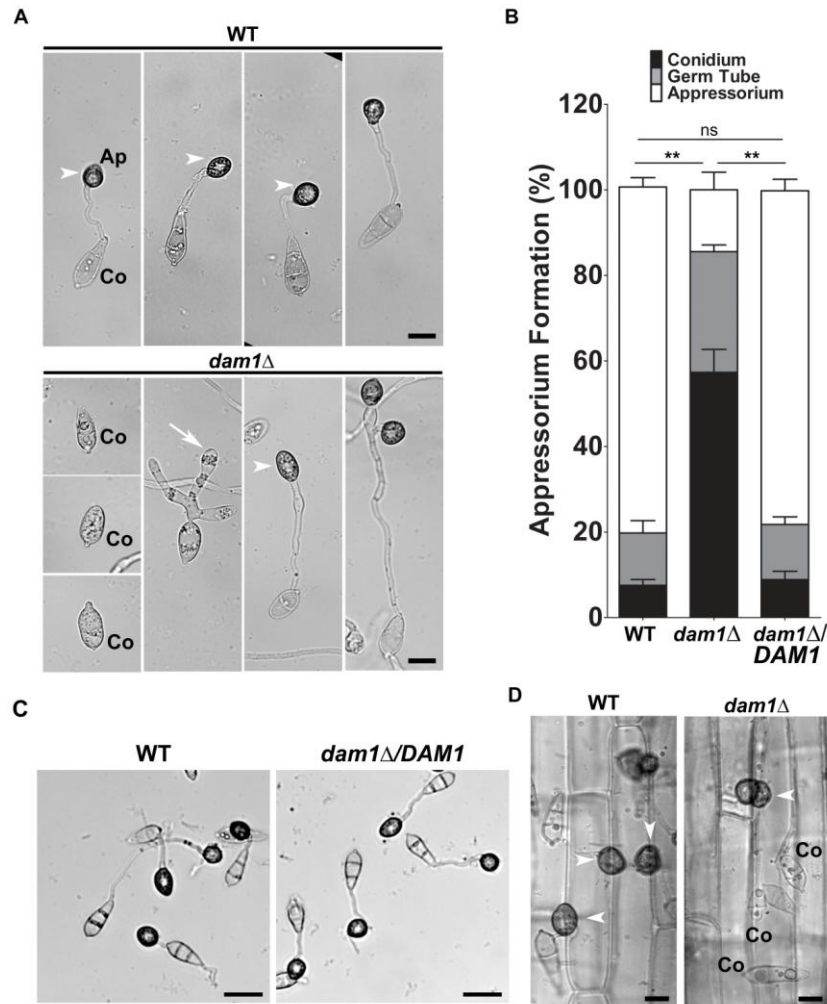


**Figure 4.21: Dam1 function is required for proper appressorium development**

A) Micrographs of pathogenic (appressorium) development in WT and *dam1*Δ strain on hydrophobic surface (glass coverslips) at 24 hpi. Arrowheads depict appressoria. Co, conidia. Scale bar = 5 μm. B) Bar chart showing frequency of appressorium formation at 24 hpi on a hydrophobic surface.  $P < 0.05$ ,  $n = 150 - 200$ . Data represent mean from three independent experiments. C) Micrographs of pathogenic (appressorium) development on hydrophobic surface (glass coverslips) at 24 hpi. Scale bar = 25 μm. D) Micrographs showing appressorium formation by complementation transformants *dam1*Δ/*DAM1* and WT conidia on rice leaf sheaths. Arrowheads depict appressoria.

In the WT, over 80% of conidia developed appressoria. In the absence of Dam1 function, only 15% conidia formed the infection structure (Fig. 4.21

A, B). A few of the mutant conidia showed atypical germ tube and/or appressorial development distinct from the single, short and non-septate germ tube that formed the mature melanised appressorium in the WT or the *dam1Δ/DAM1* complementation strain, (Fig. 4.21 A, B and C). *dam1Δ* conidia also failed to form appressoria on rice sheaths 24hpi (Fig. 4.21 D).

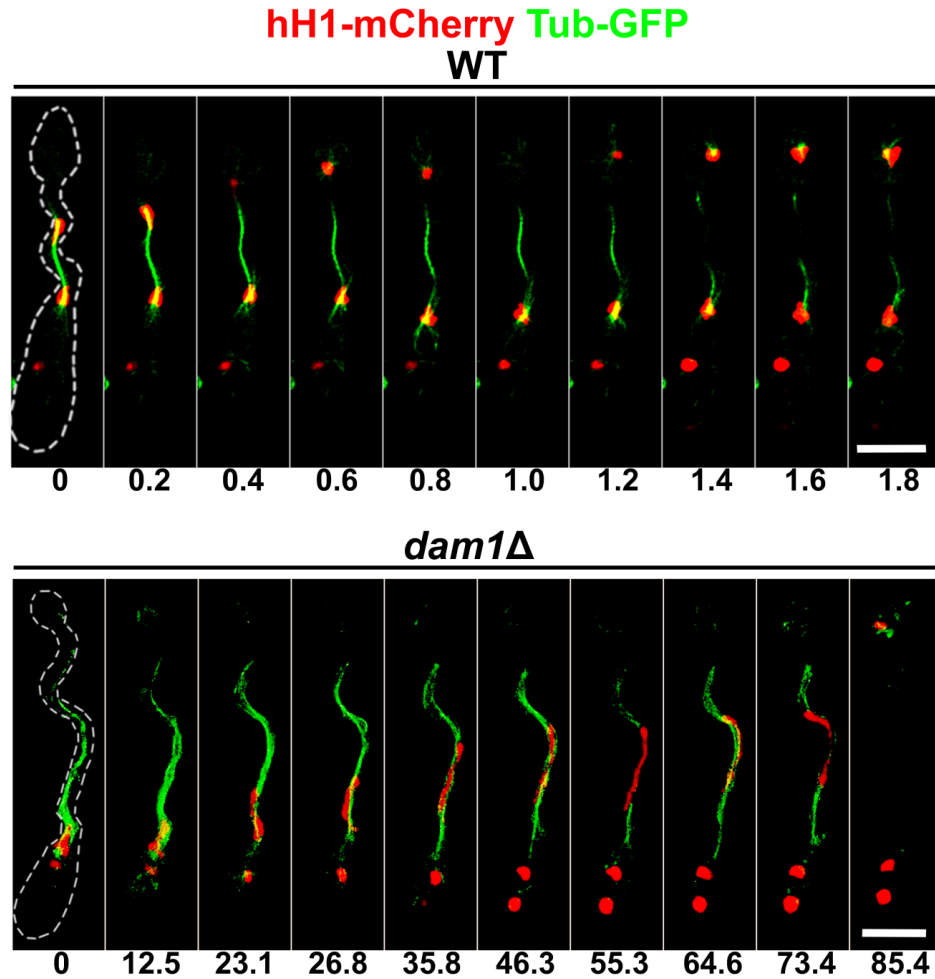


**Figure 4.22: Loss of Dam1 leads to prolonged mitosis during appressorium development**

Time-lapse images of mitosis during appressorium development in the WT and *dam1Δ* strain. Numbers indicate time in minutes. Fungal structures (conidium, germ tube and appressorium) are marked with dashed outlines. Scale bar = 10  $\mu$ m.

Completion of one round of mitosis in the germ tube is critical to appressorium development. As seen earlier in case of vegetative hyphae, mitotic progression during appressorium development is also delayed in

the *dam1* $\Delta$  mutant, and is sometimes accompanied with improper segregation of chromosomes (Fig. 4.22). The spindles were also elongated, stretching through a large part of the germ tube, and struggled to correctly segregate the nuclei and ended up as collapsed or broken spindles during appressorium development (Fig. 4.22).

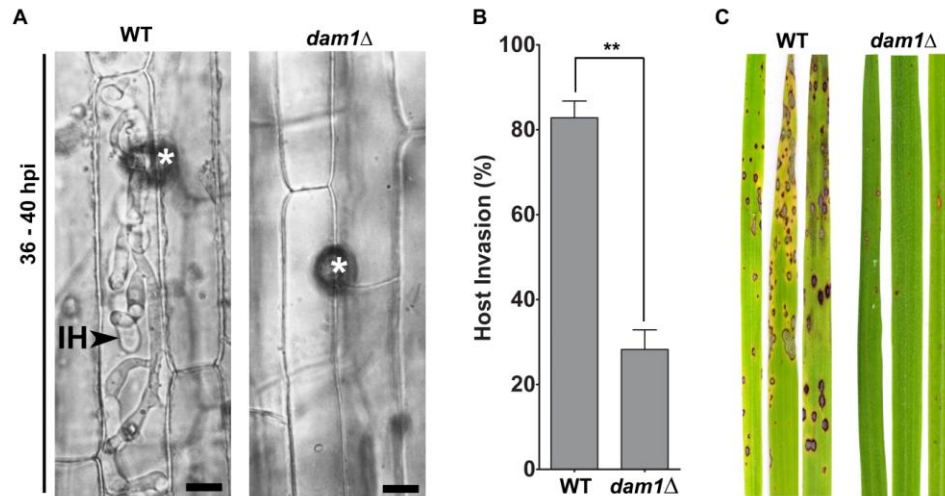


**Figure 4.23: Infection is impaired in the absence of Dam1**

A) Invasion of rice leaf sheaths inoculated with the WT or *dam1* $\Delta$  conidia and observed at 36 - 40 hpi. Arrowhead shows invasive hyphae (IH). Asterisks indicate appressoria. Scale bar = 5  $\mu$ m. B) Bar chart showing frequency of invasive hyphae at 36-40 hpi on rice leaf sheaths in the *dam1* $\Delta$  compared to the WT. \*\* $P < 0.05$ , two-tailed  $t$ -test,  $n = 100$  appressoria. Data show mean  $\pm$  S.E.M. from three independent experiments. C) Whole plant infection assay using susceptible rice variety CO-39 and  $10^5$  ml $^{-1}$  conidia of WT or *dam1* $\Delta$  strain, Leaves from inoculated plants were photographed 5 dpi. Data represent results from two independent experiments.

Unlike in the WT (over 80% penetration), rice sheath invasion 40 hpi was reduced to only 28% in case of *dam1* $\Delta$  appressoria (Fig. 4.23A, B). Ability to infect was tested on leaf tissue of an alternative host (barley) and obtained a similar result. Standard rice blast symptoms within 5-7 days were seen in the WT, while the mutant only displayed superficial vegetative growth. Further, in a standard whole plant infection assay for

WT and *dam1* $\Delta$  mutant on 3-4 weeks old susceptible CO-39 seedlings, the WT strain developed typical disease lesions 5 dpi, while the mutant displayed very low level infection with smaller disease spots sparsely distributed over the leaf (Fig. 4.23C).

*Magnaporthe* Dam1 is thus required for infection-related differentiation and plays an important role in host invasion. Host invasion by penetration peg formation requires polarised growth, nuclear division and transfer of a nucleus from the appressorium to the primary invasive hypha (Jenkinson et al., 2017). It is not clear whether the penetration and colonisation defects observed due to loss of Dam1 were purely due to improper mitotic progression or a result of its combined effect with impaired polarity of the penetration peg. Studying Dam1 sub-cellular localisation patterns during early infection stages will provide more clarity about its precise role in pathogenicity.

In the present study I have shown that two DASH complex components, Dam1 and Ask1, similar to MoDuo1 (Peng et al., 2011), are not essential for viability in *M. oryzae*, suggesting that probably more than one MT is associated with a given KT in the blast fungus, or that other protein interactions stabilise this KT-MT attachment. Single KT-MT attachment studies will shed further light on this aspect. Although there is no complete block in the cell cycle or a loss of viability in all cells within the culture, probably only a small proportion of cells are able to progress further through multiple correct rounds of mitosis. This fact may not be glaringly evident during multicellular hyphal growth but becomes particularly visible during pathogenic development both in conidiation and appressorium formation. The ability to generate *DAM1* and *ASK1* deletion mutants implies that Dam1 and Ask1 are dispensible for *M. oryzae* viability. In addition, in view of the greatly diminished capacity of *dam1* $\Delta$  to form conidia and subsequently functional appressoria that can successfully infect rice, the net ability to establish infection in the host is 2

orders of magnitude less than that of the WT. In summary, the results highlight the importance of the cell-cycle associated dynamics of outer kinetochores proteins in precise chromosome segregation and development of polarised structures critical to the asexual development and virulence of the devastating plant pathogen, *Magnaporthe oryzae*.